

Lars Røed Ramstad

Steering System and Front Suspension Development in DNV GL Fuel Fighter

Master's thesis in Mechanical Engineering

Supervisor: Knut Einar Aasland

July 2019



Lars Røed Ramstad

Steering System and Front Suspension Development in DNV GL Fuel Fighter

Master's thesis in Mechanical Engineering
Supervisor: Knut Einar Aasland
July 2019

Norwegian University of Science and Technology
Faculty of Engineering
Department of Mechanical and Industrial Engineering

NORGES TEKNISK-NATURVITENSKAPELIGE UNIVERSITET

Sammendrag

Fakultet for ingeniørvitenskap

Institutt for maskinteknikk og produksjon

Steering System and Front Suspension Development in DNV GL Fuel Fighter

av Lars Røed RAMSTAD

DNV GL Fuel Fighter er et studentlag ved NTNU, som deltar i den årlige konkurransen Shell Eco-marathon Europe. Laget bygger og utvikler kjøretøy som deltar i et kappløp mot tiden – men viktigst av alt – et kappløp mot drivstofforbruk.

Denne masteroppgaven omhandler forfatterens, og til dels andre lagmedlemmers innsats for å utvikle og konstruere et nytt styresystem og et nytt fremre hjuloppheng for lagets 2019-modell.

En literaturgjennomgang presenterer et kunnskapsgrunnlag for styresystemer, og noen av faktorene som påvirker styring. Kombinert med fastsatte konkurransekraav brukes denne informasjonen til å foreslå og evaluere fire styrekonsepter. Videre utvikling av ett av konseptene utføres, og fører til dets ferdigstillelse. På samme vis blir et nytt fremre hjuloppheng utviklet og konstruert, basert på teoretisk kunnskap fremstilt i oppgavens litteraturgjennomgang. Begge systemene ender med å bli utnyttet under Shell Eco-marathon 2019.

Til slutt gjennomgår oppgaven prosjektets grad av suksess, og effektiviteten av utviklingsprosessen i seg selv. Forslag for videre arbeid fremsettes for å kunne nyttiggjøres av neste års DNV GL Fuel Fighter-lag.

THE NORWEGIAN UNIVERSITY OF SCIENCE AND TECHNOLOGY

Abstract

Faculty of Engineering

Department of Mechanical and Industrial Engineering

Steering System and Front Suspension Development in DNV GL Fuel Fighter

by Lars Røed RAMSTAD

DNV GL Fuel Fighter is a team of students at NTNU, competing at the annual Shell Eco-marathon Europe. The team builds and designs cars that compete in a race against time – but most importantly – a race against fuel consumption.

This master thesis discusses the efforts of the author, and in part other members of the DNV GL Fuel Fighter team in developing and constructing a new steering system as well as a new front suspension and steering knuckle assembly for the teams 2019 model.

A literature review presents a knowledge base on steering systems and some of the factors that affect steering. Combined with set competition requirements, this information is used in suggesting and evaluating four steering concepts. Further development of one of the concepts is performed, resulting in its construction. Similarly, a new front suspension system is designed and constructed, based on theoretical knowledge presented in the thesis' literature review. Both systems end up being utilised at the Shell-Eco-marathon 2019.

Finally, the thesis reviews the success of the project, and the efficiency of the development process itself. Suggestion for future work are made to benefit next years DNV GL Fuel Fighter team.

Acknowledgements

First and foremost, thank you to my supervisor Knut Einar Aasland. For allowing me to be in-dependant and figuring out the direction I want to go, while still keeping an open door when I was uncertain. And also for having fostered the initiative to create the DNV GL Fuel Fighter project more than ten years ago, and working to keep it alive to this day.

Thank you to the entire DNV GL Fuel Fighter team, who have made this last year such a great experience, both in a learning perspective and a social one. Special thanks to the project administrator Eirik Furuholmen and administrative assistant Jennifer Nguyen for all your hard work organising the team; team member David Guerrero, for helping me review my own designs and aiding me in parts production; and team members Kristoffer Sydnes, Ole Andreas Wammer and Sarah Prescott for assisting me in parts production.

Thank you to employees at the Department of Mechanical and Industrial Engineering: Bjørn Martin Bendixen and Børge Holen, for assisting me with CNC production; and Øyvind Haave, for allowing me to use workshop facilities after work hours.

Contents

Sammendrag (Abstract in Norwegian)	iii
Abstract	v
Acknowledgements	vii
List of Figures	xiii
List of Abbreviations	xv
List of Symbols	xvii
1 Introduction	1
1.1 Note to the reader	1
1.2 DNV GL Fuel Fighter and the Shell Eco-marathon	2
1.2.1 Shell Eco-marathon	2
1.2.2 DNV GL Fuel Fighter	3
Organisational Hierarchy	3
1.3 Problem Description and Scope	3
2 Literature Review	5
2.1 Vehicle Reference Frame	5
2.2 Steering Systems	6
2.2.1 Ackermann Steering	6
Parallelogram Systems	7
Rack and Pinion	8
2.2.2 Steer by Wire	8
2.3 Slip Angles	8
2.3.1 Effect on Tyre Drag	9
2.4 Suspension	11
2.4.1 Suspension Components	11
Steering Knuckle	11
Suspension Arms	11
2.4.2 Suspension Setup	12
Caster Angle	12
Steering Axis Inclination	13
Camber	13
Toe	14
3 Steering System Development	15

3.1	Requirements	15
3.1.1	Regulatory Requirements	15
3.1.2	Design Requirements	16
	Physical Design Space	16
	Autonomous Operation	17
	Steering Geometry	17
3.2	Initial Idea Phase	17
3.2.1	Creating an Overview	17
3.2.2	Brainstorming	18
	Hydraulic Screw Piston	19
	Uneven Wire Pulleys	19
	Double-guide Wheel	19
	Rack and Pinion	20
3.3	Concept Elimination	20
3.3.1	Requirement Fulfilment	20
	Use of Space	20
	Power Demand	22
	Steering Geometry and Recalibration	22
	First Elimination	23
3.3.2	Feasibility	23
	Rack and Pinion	23
	Double-guide Wheel	23
	Uneven Wire Pulley	23
	Second Elimination	24
3.3.3	Decision	24
3.4	Further Development	24
3.4.1	Integration Prototype	24
	Design	24
	Testing	27
3.4.2	Concept Improvement	27
	Two-sided Wheel	27
	External Rollers	28
3.5	Defining the Guide Functions	28
3.5.1	Steering Wheel to Steering Angle Relationship	28
3.5.2	Geometry	29
	Steering Arm Length	29
	Guide Zero-point	29
3.5.3	Angle Substitution	29
3.5.4	Corrected Curve Function	30
3.5.5	Final Curve Functions	31
3.6	System Design	35
3.6.1	Steering System Placement	35
3.6.2	Material Selection and Dimensioning	36
	Material Selection	36
	High Speed Turning	36
	Standstill Turning	37
	Simulation	37

	Contact Stress	37
	Decision	38
3.7	Steering System Production	39
3.7.1	Double-guide Wheel Production	39
3.7.2	Roller Production	39
3.7.3	Mounts	40
3.7.4	Reproduction	41
4	Suspension System Development	45
4.1	Room for Improvement	45
4.1.1	Bearings	46
4.1.2	Sweep Radius	47
4.1.3	Shock Absorber	47
4.1.4	Brakes	47
4.2	Steering Knuckle Design	48
4.2.1	Material Savings	48
4.2.2	Zero Sweep Radius Design	48
4.2.3	Three Layer Concept	49
4.2.4	Spindle	50
4.3	Suspension Arms	51
4.3.1	Carbon Fibre Tube Strength Test	51
4.3.2	Suspension Arm Layout	52
4.4	Dimensioning	53
4.4.1	Load Cases	53
	High Speed Turning	53
	Maximum Power Braking	53
	Road Bump	53
4.4.2	Steering Knuckle	54
	Axle	54
	Geometric Layout	55
4.4.3	Suspension Arms	55
4.5	Suspension System Production	56
4.5.1	Steering Knuckle Production	56
	Production of the Three Layer Design	56
	Spindle Production	56
4.5.2	Suspension Arms Production	58
	Tube-ends	58
	Connectors	58
	Assembly	59
5	Results	61
5.1	Steering System	61
5.1.1	Weight	61
5.1.2	Driver Experience	62
5.1.3	Issues	63
5.2	Suspension System	64
5.2.1	Weight and Moment of Inertia	64
	Weight	64

	Moment of Inertia	64
	Total Reduction	65
5.2.2	Issues	65
6	Discussion	67
6.1	Success of Project	67
6.1.1	Steering System	68
6.1.2	Suspension System	70
6.2	Review of Process	70
6.2.1	Initial Phase	70
6.2.2	Further Development Phase	71
6.2.3	Production Phase	71
6.2.4	Conclusions	72
6.3	Future Work	72
6.3.1	Steering System	72
	Necessary Improvements	72
	Validation	73
6.3.2	Suspension System	74
	Necessary Improvements	74
	Validation	74
A	Ackermann System vs. Perfect Ackermann Geometry	77
B	Risk Assessment Form	81

List of Figures

1.1	DNV GL Fuel Fighter at the Shell Eco-marathon Europe 2018 .	2
2.1	The vehicle coordinate system, illustrated on FF19	5
2.2	Fifth-wheel steering	6
2.3	Ackermann steering	7
2.4	Parallelogram steering	7
2.5	Recirculating ball	7
2.6	Rack and pinion steering	8
2.7	Free body diagram of the “Unicycle Model”	9
2.8	Effects of speed and turning radius on tyre drag	11
2.9	Example of a double wishbone suspension system	12
2.10	Caster angle	12
2.11	Effects of steering axis inclination and camber on scrub radius	13
2.12	Toe-in vs. toe-out	14
3.1	Cross section views of drivers position in vehicle cabin	16
3.2	Extended steering column	19
3.3	Possible steering concepts	21
3.4	Implementation prototype of double-guide wheel concept (animated view)	22
3.5	Steering angles in the “Perfect Ackermann” steering geometry	25
3.6	Relationship between piston movement and steering angle	26
3.7	Integration prototype installed in FF18	26
3.8	CAD assembly of improved double-guide wheel concept (animated view)	27
3.9	Illustration of the deviation between guide curve radius and roller position	31
3.10	The four curves present on both sides of the DGW	32
3.11	Render of the front of the chassis, showing the available space in front of the dashboard	35
3.12	The double-guide wheel straight out of the CNC milling centre	39
3.13	The rollers, pins and bearings	40
3.14	Annotated render of steering system assembly	41
3.15	Indentations in the DGW	42
3.16	Remade DGW with shoulder	43
3.17	Finished steering system installed in FF19 (animated view)	43
4.1	Old suspension and steering knuckle assembly	45
4.2	Space inside the carbon fibre rim	48
4.3	Three layer steering knuckle design	49

4.4	Exploded view of spindle assembly	50
4.5	CFRP tube strength test	51
4.6	Render of suspension and steering knuckle assembly	52
4.7	Resulting Von Mises stress distribution from Abaqus study	55
4.8	FEM analysis of suspension arms	56
4.9	Finished hub mount	57
4.10	Test fitting of the axle and brake disc mount hex connection	58
4.11	An overview of the main parts of the suspension system	59
4.12	Suspension system mounted to FF19	60
6.1	The steering system seen from the FF paddock opening at SEM19	69
6.2	Sketch of the steering system with and without off-setters	73
A.1	Traditional Ackermann steering system	77
A.2	Comparison of perfect Ackermann geometry and the steering geometry of the traditional Ackermann system	79

List of Abbreviations

SEM	Shell Eco-marathon
SEM18	Shell Eco-marathon Europe 2018
SEM19	Shell Eco-marathon Europe 2019
FF	DNV GL Fuel Fighter
FF18	The DNV GL Fuel Fighter 2018 model
FF19	The DNV GL Fuel Fighter 2019 model
DGW	Double-guide Wheel
CFRP	Carbon Fiber Reinforced Polymer
Alu	Aluminium
Hex	Hexagonal
ID	Inner Diameter
OD	Outer Diameter
CNC	Computer Numerical Control

List of Symbols

α	Slip angle	$^{\circ}$
C_{α}	Cornering stiffness	$\text{N}/^{\circ}$
P	Pressure	Pa
T	Traction	N
g	Standard gravity	9.80665 m/s^2
l	Wheelbase	m
w_f	Front axle track-width	m
l_{sa}	Steering arm length	m
l_{tr}	Tie rod length	m
γ_i	Inner wheel steering angle	radians
γ_o	Outer wheel steering angle	radians
R	Outer front wheel cornering radius	m
β	Steering arm angle	radians
R	Guide curve radius	m
θ	Guide curve angle	radians
r	Roller radius	m
δ	Displacement	m
M	Bending moment	Nm
T	Torque	Nm
F	Force load	N
σ	Mechanical stress	Pa
v	Velocity	m/s
ω	Angular velocity	rad/s
m	Mass	kg
I	moment of inertia	kgm^2
KE	Kinetic energy	J

Chapter 1

Introduction

1.1 Note to the reader

This master thesis is written independently by a member of the DNV GL Fuel Fighter team. However, much of the work in the DNV GL Fuel Fighter project is done in collaboration between team members. The thesis is written in the passive form. Hence, sentences of the form “An analysis was performed...” imply that the analysis was performed by the author himself. In cases where other members have contributed, their names and their contribution is specified.

This thesis is the result of the continued work efforts from the pre-master thesis “Steering System and Load Case Development in DNV GL FuelFighter”, written by the same author in fall 2018. As much of the basis for this thesis is identical to that of the pre-master thesis, some sections are repeated in this master thesis. The pre-master thesis is a non-published document, and so this is done freely without specific reference. The pre-master thesis is uploaded as part of the submission attachment through Inspira.

This thesis details the process of development. It strives to structure sections in the most organised and comprehensible way, and so not all processes are presented in chronological order. Most of the work involved moving back and forth between different processes as new discoveries were made.

All text written in red font contains hotlinks, which directs the reader either between different sections of the document, or to external online addresses. Some figures also contain hotlinks, directing the reader to animated versions of the figures online. The external files that are referenced in these instances are also found in the submission attachment through Inspira.

Many readers prefer low light emission when reading from a screen, to prevent eye fatigue. By default this document is formatted as black text on a white background. However, if preferred for reading comfort, the document is made to support switching to light coloured text on a dark background. (In Adobe Acrobat this is done as illustrated [here](#). It’s most effective if also opting for the dark display theme, as instructed [here](#). Hotlinks remain red even as text colour is changed.)

1.2 DNV GL Fuel Fighter and the Shell Eco-marathon



Figure 1.1: DNV GL Fuel Fighter at the Shell Eco-marathon Europe 2018[21]

1.2.1 Shell Eco-marathon

The Shell Eco-marathon (SEM) is a series of competitions hosted by Shell. The events allow teams of students from all across the globe to compete on a racetrack using vehicles of their own design. There are three main events: SEM Europe, SEM Americas and SEM Asia, in addition to a series of challenger events leading up to the main regional events.[22] The competition hosts three vehicle classes: UrbanConcept, Prototype and Autonomous UrbanConcept (a new vehicle class introduced in 2018). In each vehicle class teams may choose to compete in one of three fuel classes: hydrogen fuel-cell, battery electric and internal combustion engine.[1]

In the UrbanConcept and Prototype classes, drivers are required to finish a set amount of laps around a race track within a time limit, while keeping the energy consumption as low as possible. UrbanConcept drivers are required to make a full stop during every lap. The Prototype class focuses on maximum efficiency, while the UrbanConcept class requires a more practical design in order to qualify. During SEM Europe 2018 (SEM18) the race consisted of 15 laps of 970 meters, with a maximum completion time of 35 minutes.[2]

In the Autonomous UrbanConcept class the vehicle is not controlled by a human driver, but by an autonomous system composed of perception sensors and vehicle control systems. Teams compete in navigating through a series of complicated courses. In this case, energy consumption makes up only one out of several metrics when selecting a winner.

1.2.2 DNV GL Fuel Fighter

"DNV GL Fuel Fighter" (FF) is a voluntary student organisation at NTNU, in which students from different programs of study work together to design and build highly fuel efficient road vehicles in order to compete in the annual "Shell Eco-marathon Europe". The team has been competing every year since 2008, securing a spot on the podium on several occasions, while other times not being able to finish the race.[21]

At Shell Eco-marathon Europe 2019 (SEM19), DNV GL Fuel Fighter aims to compete in the UrbanConcept vehicle class, and for the first time the Autonomous UrbanConcept vehicle class. FF intends to compete in both vehicle classes using the same vehicle, and in both cases compete in the battery electric fuel class.

Organisational Hierarchy

The team consists of five sub-teams: mechanical, electrical, autonomous, design and marketing. Additionally, there is a board consisting of the project administrator, an administrative assistant, the leaders of each sub-team and all students writing their pre-master and/or master thesis based on their FF work. The author of this pre-master thesis is represented in the board and the mechanical sub-team.

1.3 Problem Description and Scope

The vision and mission of DNV GL Fuel Fighter read as follows:

"Inspire a sustainable future - through learning and creating innovative solutions that challenge today's perception of transportation."

and

"Develop and build an ultra-efficient UrbanConcept car that excels in Shell Eco-marathon"

Achieving this is a complicated challenge, composed of many factors ranging from design and marketing to pure component and systems performance. This technical project work will seek to fulfil the vision and mission by securing the best level of performance possible for the DNV GL Fuel Fighter 2019 model (FF19), while simultaneously attempting to create inspiration and enthusiasm through unconventional solutions.

This master thesis will focus on solving two main challenges: finalising the design of a new steering system that maximises efficiency while meeting new requirements for the participation in the Autonomous UrbanConcept class,

and designing a new steering knuckle/spindle and front suspension system, which minimises mechanical losses and weight.

The development of a new steering system contributes towards the mission by attempting to re-design a system which proved to be a competitive weakness in FF18, while simultaneously attempting to inspire new and out of the box thinking in light of the vision statement. The development of the steering system is most of all an attempt to find a new solution to a problem that has already been considered solved for over two hundred years, to investigate which possibilities may arise from new solutions. The development of a new steering system is a continuation of the work effort detailed in the pre-master thesis. The steering system development is based on theoretical knowledge of steering systems presented in the literature review (2.2), as well as requirements set by the Shell Eco-marathon and the DNV GL Fuel Fighter team (3.1).

The development of a new steering knuckle and front suspension contributes to the mission by attempting to improve efficiency through reduction of weight and mechanical losses. This is done by assessing the use of light-weight materials and unconventional spindle layouts. The development is based on theoretical knowledge presented in the literature review (2.4), as well as load case data gathered through work described in the pre-master thesis.

Chapter 2

Literature Review

2.1 Vehicle Reference Frame

In order to discuss systems and components in a car, it is important to first establish a common reference frame. There are several ways to name and reference different directions and rotations with respect to a vehicle. In this thesis a coordinate system is used in which the x-axis represents the forward driving direction, the y-axis points towards the left hand side of the driver and the z-axis represents the upwards direction. In addition to this, rotation about any of these axes is named. Rotation about the x-, y- and z-axes are referred to as roll, pitch and yaw respectively. Figure 2.1 illustrates this system.

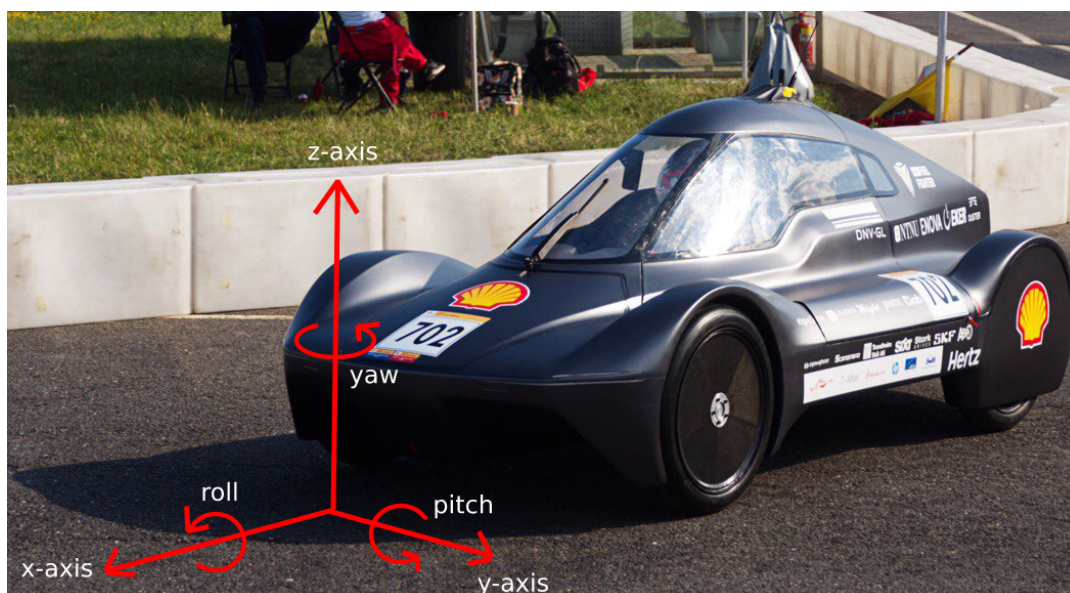


Figure 2.1: The vehicle coordinate system, illustrated on FF19.

2.2 Steering Systems

The objective of a steering system is to enable the vehicle to travel along an arc, thus rotating around a turn centre and altering the direction of travel. In other words achieving yaw. Steering a vehicle is a process that causes inherent mechanical losses. In an energy consumption challenge such as SEM it is therefore of utmost importance to minimise those losses.

2.2.1 Ackermann Steering

Traditionally, horse drawn carriages utilised a steering system in which both front wheels were fixed to a common axle. The axle was free to rotate around a pivot point at its centre, referred to as the 'fifth wheel'. This system had the advantage of both front wheels being on the same axis, and so the axis of all four wheels would always intersect in the turn centre. The axle was pivoted by the horse(s), as it was directly drawn. However, this system posed challenges for use in automotive vehicles, as the driver was required to apply large forces in order to turn the entire axle. [3, pg.305]

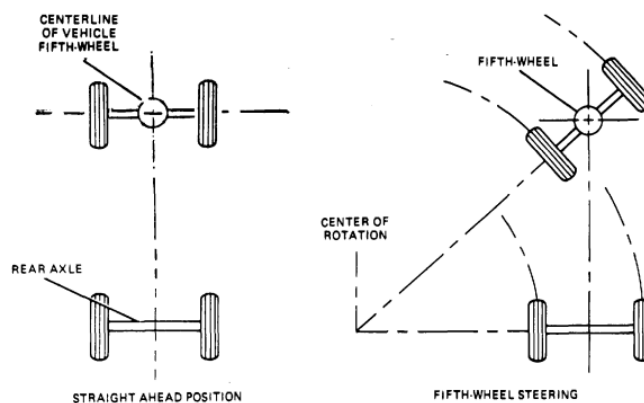


Figure 2.2: Fifth-wheel steering [4, fig.33-2]

A solution to this problem was developed in 1817, namely the Ackermann Steering system. [3, pg.305] The front wheel axis is fixed, however both front wheels are attached to a spindle that may swivel around a kingpin. Steering arms are attached to the spindles (together composing the "steering knuckle"), and a tie rod connects them. The steering arms are attached at an angle, thus the assembly forms a trapezoid. This ensures that the inner wheel rotates further around its kingpin than the outer wheel, given a certain sideways shift of the tie rod. This is referred to as a toe-out turn, as the wheels are pointed slightly apart as opposed to being parallel. [5, pg.541]

Like the "fifth wheel" systems, the intention is for all axes of all wheels to intersect in a common turn centre. This is called "perfect Ackermann steering", however, the Ackermann system itself is only an approximation and not in reality able to achieve this ideal geometry. (A)

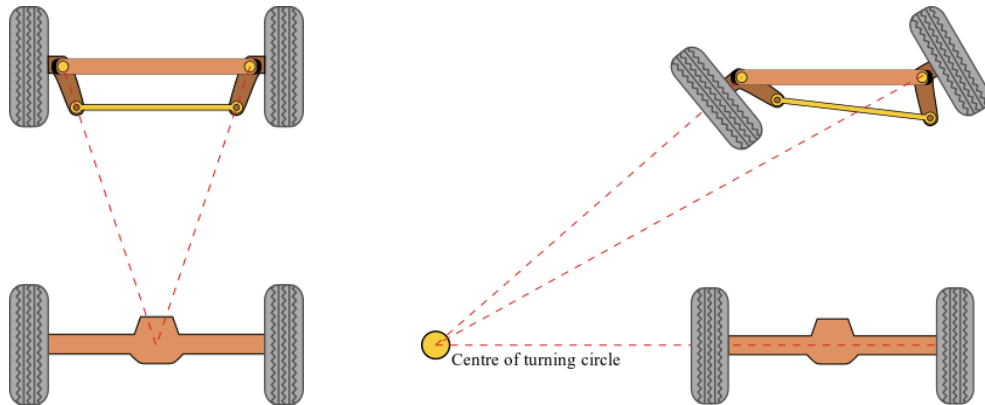


Figure 2.3: Ackerkmann steering when driving in a straight line and when turning.[23]

Nearly all cars on the market today utilise some adaption of the Ackerkmann system, however there are a number of ways it may be actualised.

Parallelogram Systems

In a parallelogram system there is one tie-rod for each wheel, connected by a centre link. The centre link is attached to two arms, the Pitman arm and the idler arm. Rotating the Pitman arm forces the centre link to shift side to side, thus steering the wheels. The Pitman arm is attached to the sector shaft, which is again driven by the steering column (connected to the steering wheel). The geared linkage between the steering column shaft and the sector shaft is named the steering box, and may be configured in a number of ways, e.g. with a worm and sector gear, worm and roller or through the recirculating ball system. The recirculating ball system is similar to a worm and sector gear, except the worm is made up of a shaft covered in bearing balls, greatly reducing the friction and therefore driver effort required to turn the steering wheel. The recirculating ball system is commonplace in large and heavy vehicles.[3, pg.308]

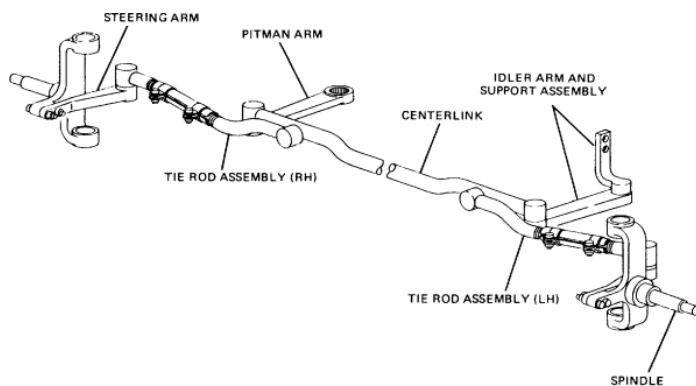


Figure 2.4: Parallelogram steering.[4, fig.33-5]

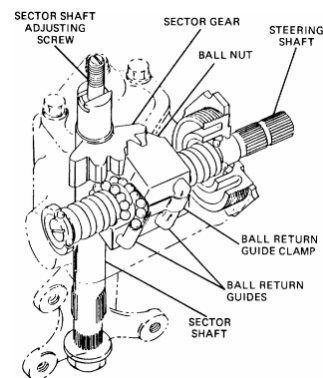


Figure 2.5: Recirculating ball.[4, fig.33-10]

Rack and Pinion

In the rack and pinion system, the centre link is mounted on a fixed path, free to move along one axis only. A tooth rack is attached directly on top of the centre link, which is in turn driven by a pinion on the steering column. Rotation of the pinion directly shifts the centre link from side to side, pushing/pulling the tie rods and turning each wheel. The rack and pinion system is simple and lightweight, in addition to providing feedback to the driver (the driver can feel forces applied to the wheels through the steering wheel), therefore it is commonly found in small vehicles and sports cars.[3, pg.308]

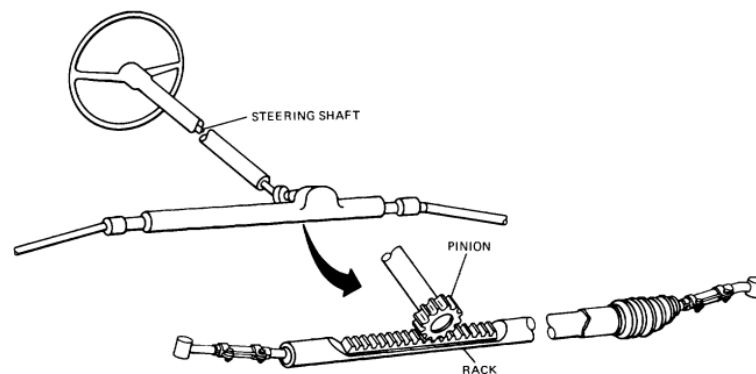


Figure 2.6: Rack and pinion steering.[4, fig.33-11]

2.2.2 Steer by Wire

As mentioned, in spite of its efforts the Ackermann system is not able to cause all wheel axis to intersect the common turn centre perfectly with varying turning radii. In addition to this, there are certain tyre deformations at speed which means it is not necessarily optimal to achieve perfect Ackermann geometry, these are discussed in 2.3. As a solution to this, some vehicle manufacturers are attempting to develop adaptive electronic steering systems, referred to as “steer by wire” systems. By allowing each front wheel to be controlled individually by electronic actuators, the vehicle control unit can provide the optimal steering angle for each wheel based on desired turning radius as well as current load, speed and tyre properties. Steer by wire systems can potentially increase energy efficiency, improve handling capabilities and improve safety, both through the enhanced handling capabilities and the absence of the steering column shaft, which is a dangerous object to have in front of the driver during a collision.[6, pg.513-526]

2.3 Slip Angles

When turning at speed, the tyres are subject to lateral forces, providing the centripetal acceleration of the vehicle. In order to generate these forces the

tyres experience some deformation, causing *slip angles*. The slip angle is the angular deviation between a wheels orientation and its direction of travel. The relationship between a wheels cornering force and slip angle may be considered linear for slip angles smaller than 5° . [3, pg.312][7]

$$F_y = C_\alpha \alpha \quad (2.1)$$

The factor of proportionality, C_α , is the cornering stiffness, and is dependant on tyre properties and load. As has been seen in the pre-master thesis, the loads on the outer wheels are larger than on the inner wheels during a turn, thus the slip angle is not equal across wheels. This effect increases with high speed and small turning radii. Adaptions in the steering geometry are often made to compensate for this. Adaptions in which the engineers aim for significantly less toe-out than with perfect Ackermann geometry are called anti-Ackermann steering, and are common in racing cars. [8]

2.3.1 Effect on Tyre Drag

The 2005 winning SEM Prototype team PAC-car II [9] performed the following analysis to determine the effect of slip angles on tyre drag when turning.

For a given tyre, the cornering stiffness was approximated by a simplified version of Pacejka's "magic formula" model [9, pg.59][10]:

$$C_\alpha = (a_{30} + a_{31}P) \sin \left(2 \tan^{-1} \left(\frac{F_z}{a_{40} + a_{41}P} \right) \right) \quad (2.2)$$

The coefficients were given for the tyre in question, and the tyre pressure was set at 6 bar, making the cornering stiffness a function of vertical load only.

The simplest way to observe tyre slip is through the "unicycle model", i.e. assuming a single wheel rolling around a turn centre in steady state.

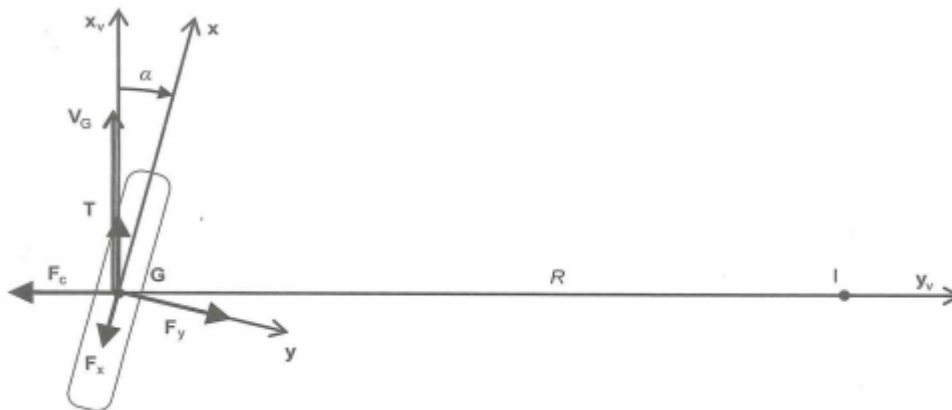


Figure 2.7: Free body diagram of the "unicycle model". [9, pg.74]

The steady state assumption defines the following equilibrium:

$$F_y \cos \alpha - F_x \sin \alpha = mv^2 / R \quad (2.3)$$

$$F_y \sin \alpha + F_x \cos \alpha = T \quad (2.4)$$

Equation 2.4 illustrates how the traction T provided to the wheel must compensate for the tyre drag to maintain steady state. The F_x component of the tyre drag represents the longitudinal component of rolling resistance in the tyres/wheels, while the F_y component represents the transverse component of the cornering force. A larger slip angle results in a larger longitudinal component of cornering force, and thus large slip angles increase tyre drag.

Assuming $\alpha < 5^\circ$, equation 2.1 holds, while $\cos \alpha \approx 1$, and $\sin \alpha \approx \alpha \frac{\pi}{180}$ (where the slip angle α is expressed in degrees).

Introducing this in 2.3 and 2.4 we get:

$$\alpha = \left(\frac{mv^2}{2} \right) / (C_\alpha - F_x) \quad (2.5)$$

$$T = C_\alpha \alpha^2 \frac{\pi}{180} + F_x \quad (2.6)$$

From 2.6 and 2.5, the tyre drag at different turning radii and velocities are plotted in figure 2.8, assuming a given vehicle mass and associated rolling resistance. The aerodynamic drag of PAC-car II is plotted alongside the tyre drag, illustrating that the tyre drag is of a significant magnitude in comparison. Bear in mind that the unicycle model produces higher slip angles than if the load was distributed on four wheels. As the tyre drag is proportional with the slip angle squared, the actual tyre drag may not be as high in a four wheel model.

However, when moving from the unicycle model to a full vehicle model, the slip angles can be “forced” higher than necessary if the steering angle relationship between the wheels is not ideal. As we have seen, high slip angles has a significant effect on tyre drag, and therefore, designing a steering system than can provide ideal steering geometry should be made a priority when efficiency is of the highest importance.

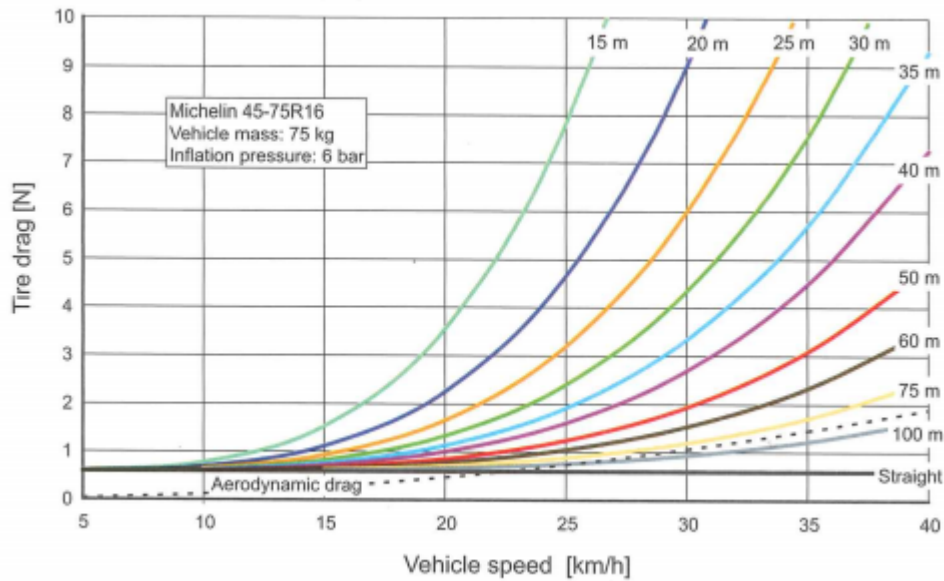


Figure 2.8: Effects of speed and turning radius on tyre drag.

2.4 Suspension

2.4.1 Suspension Components

Steering Knuckle

The steering knuckle is the part that mounts the wheel to the rest of the suspension. It is commonly called the upright, named as such because in a dampened suspension this component remains upright relative to the ground plane as the suspension moves vertically. The steering knuckle holds the wheel through the spindle, enabling the wheel to rotate. The spindle also holds the brake disk, while the steering knuckle holds the brake calipers. As the name implies, the steering knuckle can itself rotate, enabling the steering of the vehicle. The axis around which the steering knuckle rotates is the steering axis, also known as the kingpin axis. To drive this rotation, the steering knuckle also holds the steering arm, connecting it to the vehicles steering system.[5, pg.534]

Suspension Arms

There are countless types of suspension setups. This thesis is focused on the double wishbone suspension, which is prevalent in regular cars, and was used in the FF18 suspension. The system consists of two pairs of arms, holding the steering knuckle at the top and bottom end. In a dampened suspension, the arms rotate around the x-axis at both ends while a shock absorber accepts the vertical load.[3, pg.375]



Figure 2.9: Example of a double wishbone suspension system.
[24]

2.4.2 Suspension Setup

Caster Angle

Caster angle is the angle at which the steering axis is tilted in the xz -plane, (seen from the side of the vehicle). The inclusion of a caster angle is intended to add self-alignment and stability of the steering. Positive caster is defined as the steering axis inclined such that it intersects the ground in front of the wheel. This results in the tractive cornering forces in the tyre contact patch causing torque about the steering axis, which works to rotate the wheel back to the straight forward position.

Negative caster has the opposite effect. Once the wheel steers slightly off centre the tractive forces will create torque around the steering axis in the opposite direction, causing the wheels to steer more. A simple demonstration of this is holding a bicycle by the seat and attempting to push it forward, then backwards. In the first case the fork has positive caster, making the wheel

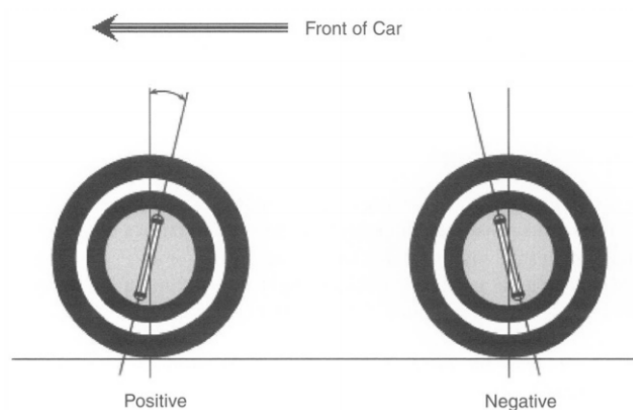


Figure 2.10: Caster angle. [3, Fig.7.21]

self align and thus the bike can easily be pushed without holding the handle bars. In the latter case the wheel will quickly turn 90 degrees, and be dragged along the ground.

Steering Axis Inclination

Steering axis inclination is the angle at which the steering axis is tilted in the yz-plane (seen from the front). The objective of steering axis inclination is to reduce scrub radius – the radius at which the tyre is being dragged around the steering axis when turned. A high scrub radius results in a large driver effort to turn the wheels, and increased tyre wear. [11, pg.499]

Additionally, steering axis inclination has some self-centring effect. When turning, the wheel is pushed down towards the ground due to the inclination, which lifts the vehicle upwards. When letting go of the steering wheel, the weight of the vehicle will act to turn the wheels back to the straight forward position.

Camber

Camber is the angle of the wheels own rotational axis in the yz-plane. Positive camber is defined as when the top of the wheel is tilted away from the vehicle. Negative camber is when the top of the wheel tilts towards the vehicle. A positive camber is used in vehicles with narrow tyres of high diameter, to reduce the scrub radius in the same way steering axis inclination does. In newer vehicles with wide tyres of smaller diameter however, camber is usually adjusted so that it will be close to zero when the car is in motion, to increase the tyre contact patch.[11, pg.497]

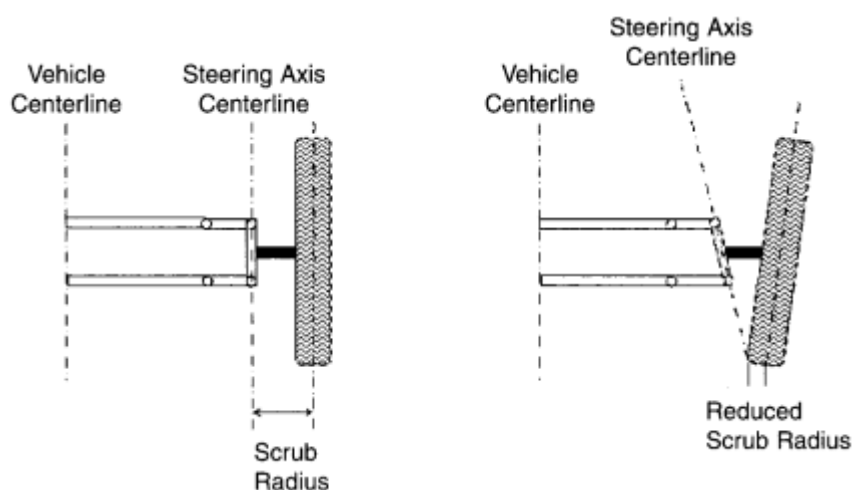


Figure 2.11: Effects of steering axis inclination and camber on scrub radius. [3, fig.7.18]

The Pac car II team performed an experiment comparing the rolling resistance coefficient of a negative camber setup and a zero camber setup. Their

results showed a 25% increase in the rolling resistance coefficient of their tyre setup, when adjusting the camber angle from zero to -4° . They did however see an increase in stability.[9, pg.67]

Toe

Toe is the difference in angle between the rotational axes of the two wheels in the xy-plane. Toe-in refers to the front end of the wheels pointing towards each other, while toe-out refers to the front end of the wheels pointing apart from each other. Toe is undesired when driving straight forwards, as the wheels are not perfectly aligned with their direction of travel, but rather sliding slightly sideways.

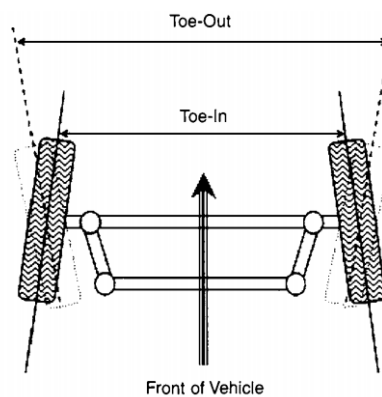


Figure 2.12: Toe-in vs. toe-out. [3, fig.7.20]

Toe causes mechanical losses and unnecessary tyre wear. Still, most vehicles are designed with a slight amount of "static toe". Whenever a scrub-radius is present, the rolling resistance (or alternatively traction in a front wheel drive vehicle) will cause torque around the steering axis. Since there will always be a certain amount of play, component deformation, and wear in any system, this torque would cause toe if left uncorrected. The static toe is therefore set to compensate for the toe induced by rolling resistance or tyre traction when driving.[11, pg.500]

Chapter 3

Steering System Development

3.1 Requirements

3.1.1 Regulatory Requirements

ARTICLE 47: TURNING RADIUS AND STEERING

- a) Vehicle steering must be achieved by one system operated with both hands using a turning motion. It must be precise, with no play or delay. Steering must be operated predominately through the front wheels.
- b) Steering must be achieved using a steering wheel or sections of a wheel with a minimum diameter of 250 mm.
- c) Steering bars, tillers, joysticks, indirect or electric systems are not permitted.
- d) The turning radius must be 6 m or less. The turning radius is the distance between the centre of the circle and the external wheel of the vehicle. The external wheel of the vehicle must be able to follow a 90° arc of 6 m radius in both directions. The steering system must be designed to prevent any contact between tyre and body or chassis.
- e) The Organisers reserve the right to set up a vehicle handling course to verify the following when the vehicle is in motion: driver skills, turning radius and steering precision.

-Shell Eco-marathon 2019 Official Rules[1, pg.21]

Seen are the steering system requirements set by Shell for the 2019 Eco-marathon. Note particularly that the rules do not allow the use of electric steering systems, such as the steer by wire systems discussed in 2.2.2. The requirement of achieving a turning radius of 6 meters or less defines the required maximum steering angle for a given set of vehicle dimensions. The requirement of

avoiding contact between tyres and vehicle body in turn defines the required wheel well dimensions.

3.1.2 Design Requirements

In addition to the requirements set by Shell, there are a number of internal requirements and constraints to be met when designing a steering system.

Physical Design Space

Figure 3.1b displays a cross section of FF19, with a driver, illustrating how the legs of the driver consume space between the front wheels. Shell Eco-marathon 2019 Official Rules states:

Article 30 a)

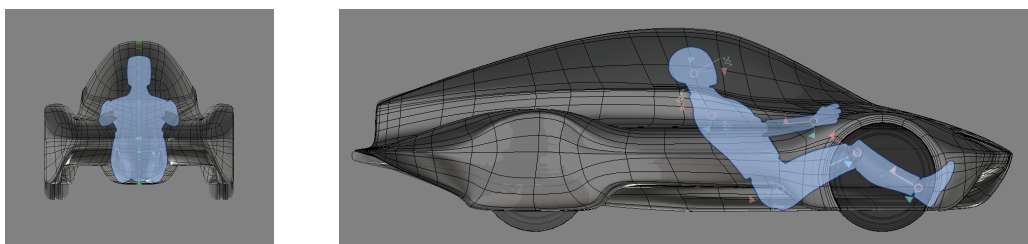
It is imperative for Drivers, fully harnessed, to be able to vacate their vehicles at any time without assistance in less than 10 seconds. [1, pg.16]

With this in mind it was made a priority for the steering system to avoid being excessively intrusive of the space occupied by the driver when operating and entering/exiting the vehicle.

Figure 3.1a displays another cross section of the chassis. Notice how the floor of the body curves up between the wheel wells and the centre of the driver's compartment. A traditional steering system usually occupies the space in a direct line between the hubs of the two front wheels, which in this case involves penetrating through the chassis in the curved sections. However, in light of article 46 b) in the official rules, this is not an option for FF19.

Article 46 b)

The vehicle body must cover all mechanical parts when viewed from all sides. The wheels and suspension must be fully covered by the body when seen from above, and the wheels must be covered up to the axle centre line when seen from front or rear. The covering for the wheels and suspension must be a rigid, integral part of the vehicle body. [1, pg.21]



(a) Front view.

(b) Side view.

Figure 3.1: Cross section views of the drivers position in vehicle cabin.

In addition to these factors, a dashboard and a braking system that will be installed in the drivers compartment are not displayed in the figures, and contribute to further limiting the space available for steering design.

Autonomous Operation

In order to compete in the Autonomous UrbanConcept class, the steering system must be operable without driver input, i.e. with the use of electronic actuators.

This involves making the necessary space and mounts for the actuator, and ensuring that the operation of the steering does not require a too high amount of power. If the steering becomes very power demanding, this will impact both the electrical power consumption directly, as well as indirectly, following the need of a large and powerful actuator.

Steering Geometry

As discussed in 2.2, an efficient steering system requires a different steering angle on each wheel, to ensure that the transverse tyre forces do not have an unnecessarily large component opposite of the direction of movement. The widely used Ackermann system attempts to accomplish this, although it never reaches “perfect Ackermann geometry”. Appendix A shows that in the case of FF19 the maximum deviation between the traditional Ackermann system and perfect Ackermann geometry is 1.52° . As seen in 2.3.1, even small slip angles have a significant impact on rolling resistance. Yet, adjusting the steering arm angle could achieve much smaller deviations, even with a traditional system. Steer by wire systems are able to accommodate any desired combination of steering angles, however, as illustrated in 3.1.1, these are not allowed in competition.

Driven by the DNV GL Fuel Fighter’s vision statement – to inspire through innovative solutions that challenge today’s perception of transportation – there was a desire for the design of a mechanical system that allowed itself to be calibrated to any desired combination of steering angles. This turned out to be a highly consuming priority in the following design process.

3.2 Initial Idea Phase

3.2.1 Creating an Overview

The idea phase started with only the most conspicuous requirement in mind – the system needs to translate the turning motion of the steering wheel into the turning motion of the two front wheels. Thus began a review of every motion translation device palpable. These were divided into two categories:

- Those initiated in the contact patch of two mediums
 - Spur and helical gears
 - Bevel and worm gears
 - Lead screws
 - Levers and links
 - Pulleys
 - Rails/guides
 - Flexible couplings
- Those conducted through a medium over a distance
 - Wires
 - Shafts
 - Flexible shafts
 - Hydraulic tubes
 - Chains
 - Belts

Some of these devices immediately stood out, both in a negative and positive fashion. E.g. bevel and worm gears produce high amounts of friction[12, pg.714], which increases the power required for autonomous operation (the exception to this being recirculating ball type worm gears, as discussed in 2.2.1). Wire and hydraulic systems, on the other hand, were seen in a positive light, as they can easily translate motion between completely different locations and orientations, thus allowing the designer to limit the use of space in crowded locations in the drivers cabin.

In order to achieve different steering angles for each wheel with a given angle of the steering wheel, there needs to be a non-constant translation ratio between components. Traditional gears can not achieve this without changing the gears, while e.g. rails and guides, belt and wire pulleys and chain sprockets are able to do this continuously by varying their shape. Alternatively, as in the Ackermann system, sets of levers and links can also achieve non-constant translation ratios. One might also consider that worm gears or lead screws could produce variable translation ratios by varying the thread pitch along their length. However, it is not obvious how such a component might be produced.

3.2.2 Brainstorming

Based on the overview presented in 3.2.1, sets of ideas were conceptualised and sketched. Figure 3.2 illustrates an idea to extend the steering column

from the steering wheel all the way to a steering box in the nose of the vehicle, where space is more plentiful, allowing wires or hydraulics to translate the motions rearwards to the wheels. Detailed in this sub-section are the concepts that received the most attention, some of which are based on the idea illustrated in figure 3.2.

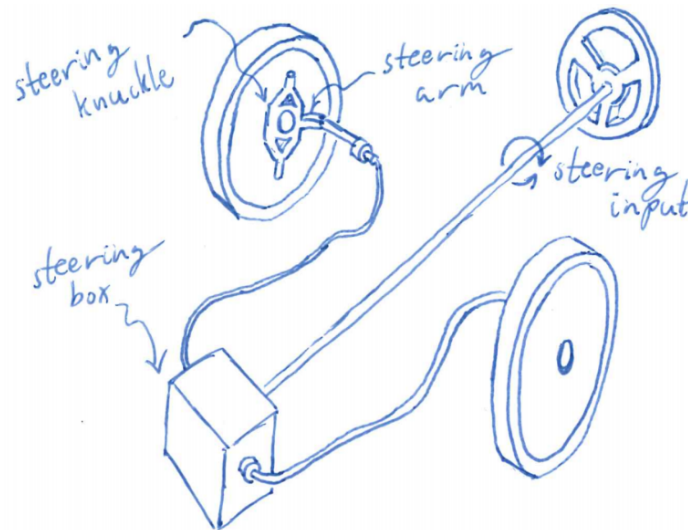


Figure 3.2: Extended steering column.

Hydraulic Screw Piston

The steering column drives a screw into an hydraulic cylinder. This concept could be used in one of two ways: a single hydraulic screw piston could drive a traditional Ackermann system centre link side to side; or, by fabricating two sets of screws and pistons with variable thread pitch one could allow individual angling of each wheel as desired. A major part of the idea was for the pistons to be transparent, and clearly visible in the drivers cabin, thus making them a design feature.

Uneven Wire Pulleys

This concept based itself off of an idea by project administrator Eirik Furuholmen. A double set of unevenly shaped pulleys attached to the steering column drives wires that turn the wheels individually. The shape of the pulleys define the translation ratios and thus the steering geometry.

Double-guide Wheel

The double-guide wheel (DGW) system consists of a wheel attached to the steering column, in which two grooves are made. Each groove guides a linear piston in or out when the steering wheel is turned. From there, each of

the linear pistons drives either wires, hydraulics or “tie-rods” (see 2.2.1) to the steering arms of each of the front wheels. The radial distance from the centre of the double-guide wheel to the groove at any given angle defines the steering angle of the wheel it controls.

Rack and Pinion

In addition to developing these new concepts, the rack and pinion steering system used in FF18 was assessed for possible reuse. In FF18, the rack and pinion was floor-mounted between the two front wheels. However, as seen in 3.1a, use of this space is limited. The steering arm of the steering knuckle in the suspension system can theoretically be extended vertically to any height within the rim of the wheel. Looking at 3.1b, there appears to be space between the wheels in what represents the first quadrant of the wheel circle in that view, over the driver’s ankles. Hence, if extending the steering arm vertically to that position, the rack and pinion could be mounted from the top down, instead of on the floor. This will also serve the advantage of not interfering with the braking pedal and cylinder layout. This positioning will require the driver to pull his/her legs out from underneath the centre link of the steering system when exiting the vehicle, hence it does complicate the fulfilment of Article 30 a)[1, pg.16], discussed in 3.1.2.

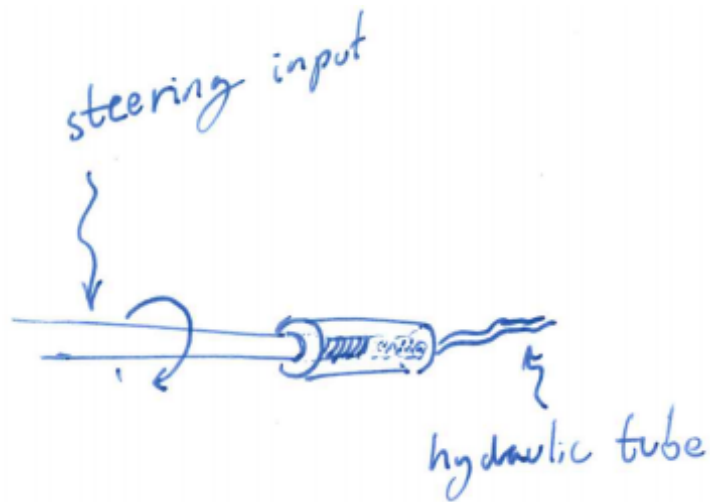
3.3 Concept Elimination

There was insufficient capacity within the team to enter into detailed design of all four concepts. However, inspired by set-based design principles ([13]), there was also reluctance towards simply choosing the most attractive concept and continue development. Instead, the concepts were subject to two iterations of consideration, in order to eliminate concepts from the bottom up.

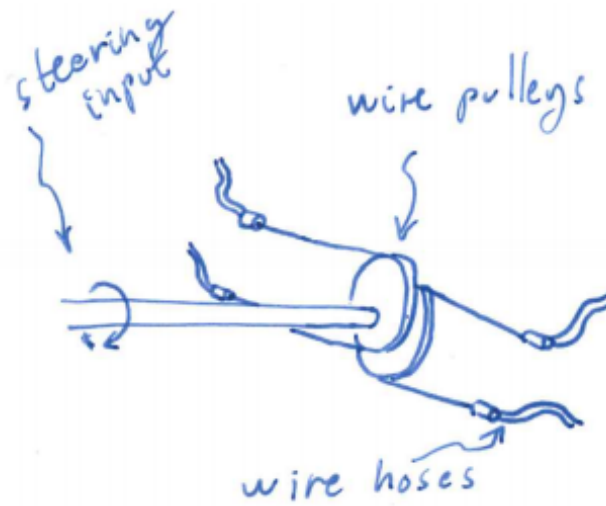
3.3.1 Requirement Fulfilment

Use of Space

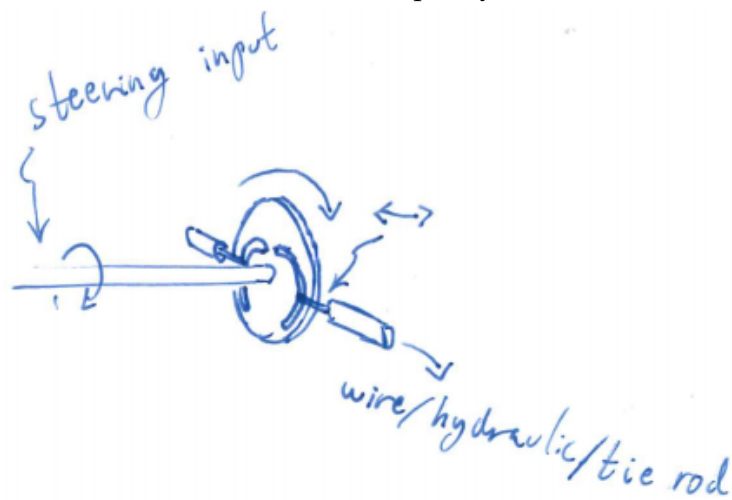
The four concepts were evaluated based on their ability to fulfil the requirements discussed in 3.1. In terms of use of space, the uneven wire pulley system, and the double-guide wheel systems scored highly, as they could be positioned anywhere and translate motion to the wheels through wires or hydraulics. The hydraulic screw piston system had the same advantage, given the second of the two proposed configurations, in which there are two pistons, one for each wheel. The first configuration of the hydraulic screw piston and the rack and pinion system from FF18 both suffered the disadvantage of requiring space in-between the wheels.



(a) Hydraulic screw piston.



(b) Uneven wire pulleys.



(c) Double-guide wheel.

Figure 3.3: Possible steering concepts.

Power Demand

Considering the use of electronic actuators to power the steering, the concepts were evaluated in terms of assumed power demand. The uneven wire pulley concept was assumed to be operable with low power, and experience dictated the same for the rack and pinion system. The hydraulic screw piston concept on the other hand fell short, as threaded connections are known to produce high amounts of friction, especially under pressure.[12, pg.714] To reduce the friction, the radius of the piston would need to be large, requiring more space, and resulting in higher weight. Scepticism existed as to whether the double-guide wheel system could operate smoothly, and so a decision was made to create a simple implementation prototype[14, pg.376] to validate the concept.



Figure 3.4: Implementation prototype of double-guide wheel concept. [\(click the figure or caption to see a motion animation\)](#)

A model was created in CAD, consisting of a frame, a wheel with carved out guides, and two pistons with pins that glide along the guides. The assumption being that if a small-scale simple FDM prototype with poor surface finish, loose tolerances and pins that glide along the guides could operate smoothly, then so would a full scale, smoothed component with guide rollers. The results were in fact validating. A model showed surprisingly smooth operation at first attempt.

Steering Geometry and Recalibration

Finally, the degree to which the concepts could provide ideal steering geometry and recalibration was assessed. The rack and pinion concept works by the Ackermann steering design, and is known to only approximate the perfect Ackermann steering geometry. The steering geometry can be adjusted by changing the length and angle of the steering arms, and recalibrated if these parts are made adjustable. In the case of the existing system from FF18, they were not. The uneven wire pulley concept and the double-guide wheel concept both allow the designer to achieve the exact desired steering geometry. Furthermore, the geometry is in both cases defined by a single component

only, the pulley/wheel, and so the steering geometry can be completely re-defined by changing only that single component. Finally, the hydraulic screw piston could potentially utilise the geometry of the rack and pinion system, or define its own. But in the latter case, both the two pistons and their screws would need to be redesigned and remanufactured in order to recalibrate the steering geometry.

First Elimination

Based on the first round of assessment, the hydraulic screw-piston appeared to be the weak link. Not only did it not deliver well in terms of the set requirements, but additionally it appeared unnecessarily complicated, with no apparent advantage over the other concepts. Except perhaps for the prospect of being utilised as a design feature. Subsequently, the concept was eliminated.

3.3.2 Feasibility

Rack and Pinion

The three remaining concepts were evaluated in terms of how easily they could be designed, manufactured and assembled in FF19. The rack and pinion system from FF19 was of course already designed and manufactured. As described in 3.2.2, based on CAD models there appeared to be sufficient space to mount the system in FF19, though it would likely be a sub-optimal fit.

Double-guide Wheel

The double-guide wheel concept was assessed to be easily designed and manufactured. The steering angle of each wheel is determined by the radius of the groove at any angle of the steering wheel. Simple trigonometry is all that is required to go from a desired steering angle relationship and the design of the steering guides. The wheel could be CNC-milled with a regular three-axis machine, and the pistons could be bought from a supplier.

Uneven Wire Pulley

Determining the shape of the uneven wire pulley to produce a desired set of steering angle ratios is more computationally demanding. The point of tangent between the wires and the pulleys move as the pulleys rotate when they are of an uneven shape. Thus, not only does one need to consider the radius at any angle, but also the accumulated path-length along the pulley up until

the moving tangent point. However, once designed the pulleys themselves could probably be easily manufactured in a three-axis CNC-mill.

Second Elimination

The assessment concluded that the rack and pinion system from FF18 served strong advantages by already being built and proven functional. An adaptation of the existing system for FF19 would therefore be a low risk solution demanding low effort. The double-guide wheel served strong advantages in being able to work with either wires, hydraulics or tie-rods, providing full control of steering geometry, and not necessarily demanding use of space between the wheels. The uneven-pulley system promised nearly the same, with the exception of excluding the possibility of using hydraulics or tie-rods. The combination of being more complicated to design and showing no other apparent major advantages led to the uneven pulley concept being shelved.

3.3.3 Decision

Based on the findings a strategy was selected: to continue development on the double-guide wheel concept, while adapting the old rack and pinion system for installation in FF19 as a fail-safe. The major piece of justification for not fully abandoning the rack and pinion system was risk mitigation. Even though the rack and pinion system from FF18 is by no means optimal, it is proven functional. Starting development of a brand new concept is always a risk in itself, with a vast amount of unknowns. Attempts were made to search for similar applications of the mechanism used in the double-guide wheel concept online, with no success. Thus, attempting to design an unproven concept under time pressure, with no back-up solution was considered reckless. After all, in a competition like the Shell Eco-marathon, a barely working design on time is better than an optimal solution one day late.

3.4 Further Development

3.4.1 Integration Prototype

Design

In order to further validate and improve the concept, testing was needed. Therefore design was initiated on an integration prototype[14, pg.377] for FF18, so that it could be used in testing while FF19 was being built. The following criteria were set:

- Allow a 6 m outside wheel turning radius, in accordance with SEM requirements.[1, pg.21]

- Maintain a linear relationship between the turning angle of the steering wheel, and the steering angle of the inner wheel.
- the system should be compatible with the tie rods and steering knuckles already mounted in FF18.

The linear movement of the pistons required to produce a given steering angle was determined through simple trigonometry. The same goes for the steering angles for any steering radius, assuming perfect Ackermann steering. These relationships allowed the radius of the guide in the double-guide wheel to be determined at every angle.

The absolute dimensions of the double-guide wheel mechanism is somewhat arbitrary, a larger wheel results in a lower guide radius gradient, and in turn smoother operation. The size needed for satisfactory operation needs to be determined by experience. For the purpose of this prototype, a 20 cm outer diameter was selected, this leaves a bare minimum of space between the guide and the centre of the guide-wheel at the smallest radius. For the two guides not to interfere with each other, less than 180° of the wheel is available to each guide, meaning the 6 m turn radius must be achieved within 90° rotation of the steering wheel.

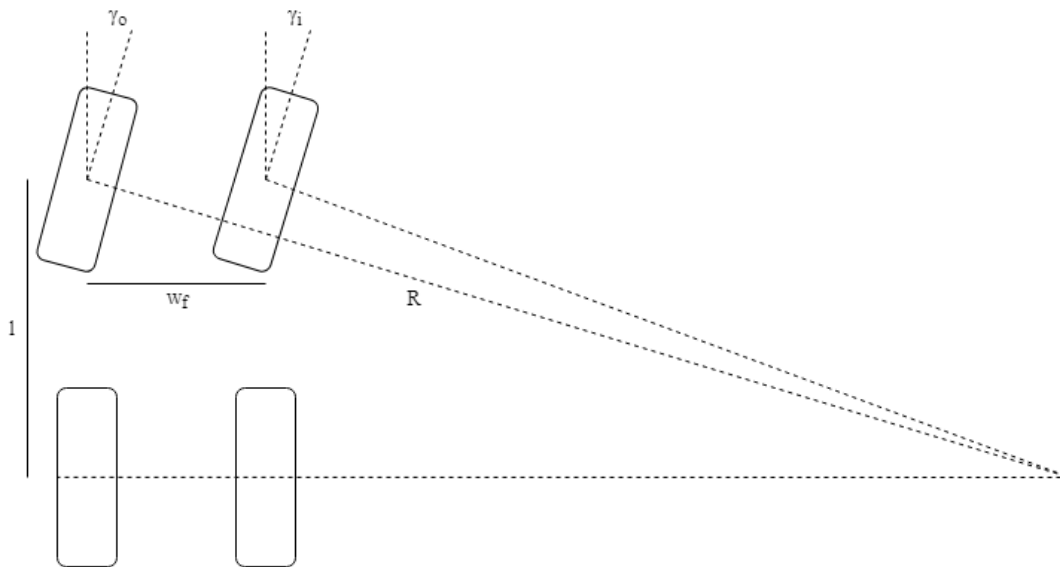
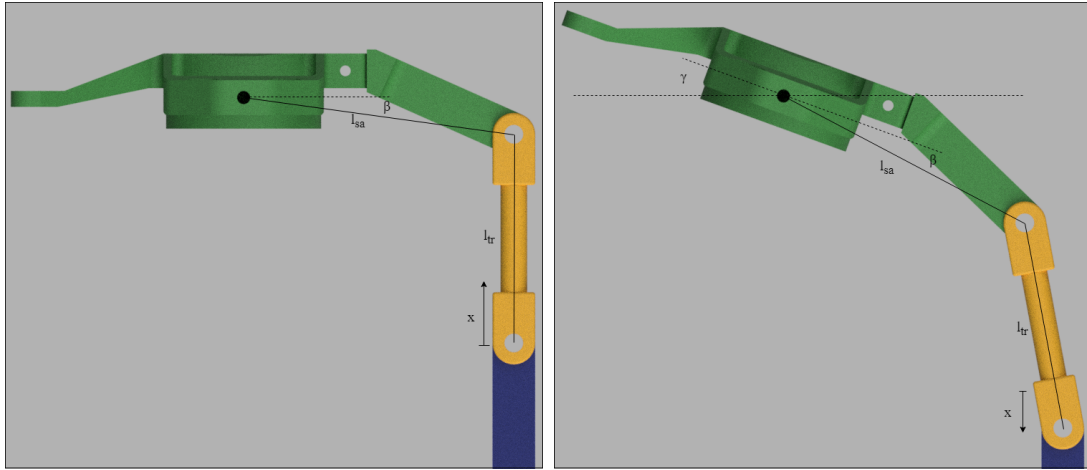


Figure 3.5: Steering angles in the “perfect Ackermann” steering geometry.

$$\gamma_i = \tan^{-1}\left(\frac{l}{\sqrt{R^2 - l^2} - w_f}\right) \quad (3.1)$$

$$\gamma_o = \tan^{-1}\left(\frac{l}{\sqrt{R^2 - l^2}}\right) \quad (3.2)$$



(a) Driving straight.

(b) Turning.

Figure 3.6: Relationship between piston movement x and steering angle γ in FF18 (steering knuckle in green, tie-rod in yellow, piston in blue).

$$x = l_{tr} \left[1 - \cos \left(\sin^{-1} \left(l_{sa} \frac{[\cos(\beta) - \cos(\beta + \gamma)]}{l_{tr}} \right) \right) \right] - l_{sa} [\sin(\beta + \gamma) - \sin(\beta)] \quad (3.3)$$

Design was performed in Autodesk Inventor Professional, using polar function curve features. There are two symmetrical guides, one controlling each wheel. Each guide consists of two halves, one half controls the steering when the corresponding wheel acts as the inner wheel, and the other half when the wheel acts as the outer wheel. The first half of the curve is controlled by equation 3.3, where γ is substituted by γ_i . In the other half of the curve γ is substituted by γ_o as a function of γ_i . Thus, at any angle of the steering wheel the system provides different steering angles to each wheel, coherent with perfect Ackermann steering geometry. More details regarding how these curve function are made is discussed in 3.5



Figure 3.7: Integration prototype installed in FF18.

External Rollers

Additionally, a realisation was made that the guides could rather be made out of “ridges” with rollers on each side, in stead of grooves with rollers inside. This would make the wheel itself much thinner, and thereby save weight, in addition to removing the issue of making the rollers compact enough to fit inside the grooves. It also removes the need to keep excess space in the groove, so that the internal roller can roll along one side without rubbing against the other. With one roller on each side of the guide, both can be in constant contact with the grooves, rolling in opposite directions, and reducing play in the system.

3.5 Defining the Guide Functions

The functions defining the guides was constructed for FF19 in the same way it was for the integration prototype used in FF18, except the steering arm now being directed to the front of the vehicle, reversing the sign. The front axle track width of FF19 is 1115 mm, and the wheelbase is 1745 mm. Using 3.1, we find that in order to achieve the required 6 m radius turn, the inside wheel needs a steering angle of 20.7°. For extra assurance it was decided to aim for a 5.5 m turning radius, thus an inner wheel steering angle of 23.1° is needed.

3.5.1 Steering Wheel to Steering Angle Relationship

The steering wheel used in FF19 consists of two grip sections instead of a full wheel, thus letting go of the wheel for multiple rotations would be uncomfortable. Therefore the 23.1° (0.40 rad) inner front wheel steering angle must be achieved within 180° (π rad) rotation of the steering wheel. The curve functions are defined in Autodesk Inventor as parametric functions in polar coordinates. The angle θ is defined as $\pi/0.40 \text{ rad} * t$ with t ranging from 0 to 0.4 rad, the relationship between turning of the steering wheel and the turning of the inner front wheel. This results in a linear relationship between the angle of the steering wheel and the steering angle of the inner front wheel, however another relationship could have been chosen if so desired. The radius R at a given point along the curve is defined by function 3.3, in which the steering angle γ is substituted by the parametric variable t. This is the same variable used in the expression for θ . Thus, for any given desired inner wheel steering angle the function will determine a radius and an angle along the guide curve that would move the pistons to the corresponding position, ensuring that the given steering angle occurs at the corresponding steering wheel angle.

3.5.2 Geometry

Steering Arm Length

The length of the steering arm defines how large the range of movement of the guides need to be. Given the height of the placement of the steering system, detailed in 3.6.1, the steering arms needed to clear the edge of the rim in the transverse direction. This meant the arms needed a 65 mm coefficient in the transverse direction (y-axis in the vehicle coordinate system). The length of the steering arms in the longitudinal direction (x-axis) however, could be chosen freely.

Inside the wheel well of the carbon fibre monocoque are foam inserts, meant to strengthen the structure in the areas at which the suspension is meant to be mounted. To clear the foam reinforced section, the steering arms would need to be at least 80 mm long in the x-direction. At 100 mm long in the x-direction, the travel of the guides would need to be 66 mm. The amount of travel sets the minimum radius of the guide wheel, a large radius means lower slope of the guides, thus lower driver effort. However, a too large radius will take up a high amount of space. Cardboard "wheels" of different sizes were held in the position in which the double-guide wheel was set to be mounted, while the driver sat in the vehicle. The maximum size at which the driver was still comfortable not interfering with the wheel was selected, resulting in a steering arm length of 100 mm in the x-direction, and kept at 65 mm in the y-direction. The steering arm height was set to reach the level of the dashboard, where the steering system would be mounted (3.6.1).

Guide Zero-point

The guides need to start at a common zero-point. Rotate the steering wheel one direction, and the relevant side of the guide pushes/pulls the steering arm to steer in a given direction; rotate the other way and the opposite side of the guide pulls/pushes to steer in the opposite direction. The amount of travel of the guide was set by the desired minimum turn radius and steering arm length. As the side of the guides that pull the steering arms spiral towards the centre of the guide wheel, the zero point needs to be placed at an adequate radial distance from the centre to allow sufficient space. In this case the zero point was set at 55 mm, allowing 16 mm of clearance between the inwards spiralling guide section and the steering column at the centre of the guide wheel. This resulted in a maximum radius of the guide of 102 mm.

3.5.3 Angle Substitution

With the steering arm directed in the forwards direction (3.6.1), the outwards spiralling section of the guide steers the inner wheel during a turn by pushing its steering arm. The amount of steering is already defined as linearly

dependant of the steering wheel angle (3.5.1). The inwards spiralling section steers the outer wheel, and as explained in 2.2.1, its angle should be controlled relatively to the steering angle of the inner wheel, by the perfect Ackermann geometry. Combining 3.1 and 3.2 we get:

$$\gamma_o = \tan^{-1}\left(\frac{l}{\frac{l}{\tan(\gamma_i)} + w_f}\right) \quad (3.4)$$

By substituting the steering angle in the same guide function used for the inner wheel by equation 3.4, we get an outer wheel curve function which provides the corresponding steering angle to the outer wheel.

3.5.4 Corrected Curve Function

The construction of the integration prototype (3.4.1) caused awareness of the fact that as the gradient of the guides changes along the curve, the effective width of the guides along the radial direction changes as well. At the smallest radii the space between the guides is at it's smallest, and the roller was pinched in between the guides. At the highest radii of the guide the space between the guides were large enough to cause a high amount of "wobble room" for the roller. This issue was in need of correction.

The numerical derivatives of the curve functions defining the guides was found through the help of the online plotting tool GeoGebra. A linear approximation of these derivatives was used, to keep the guide functions from becoming too large and difficult to handle when working in Inventor. The linear approximations are given as:

$$dR/d\theta \approx 45.0\theta - 100.3 \quad (3.5)$$

$$dR/d\theta \approx 148.5\theta - 100.3 \quad (3.6)$$

for the inner and outer wheel respectively. The angle of the guides tangent at a given point was then determined as $\tan^{-1}\left(\frac{*guide\ derivative*}{*guide\ radius*}\right)$.

Figure 3.9 illustrates how the angle of the guide causes interference between the guide and the roller. In order for the roller to position itself at the correct radial distance from the guide wheels centre at a given angle, the guide curve must be shifted by the distance $\delta = \frac{r}{\cos(\alpha)} - r$. Thus, in its entirety the curve correction function subtracts or adds:

$$\delta = \frac{r}{\cos\left[\tan^{-1}\left(\frac{dR/d\theta}{R}\right)\right]} - r \quad (3.7)$$

where $dR/d\theta$ is the linear approximation of the derivative of the guide function, given by 3.5 or 3.6, and R is the radius of the guide at the given angle, given by the guide function itself (prior to the correction).

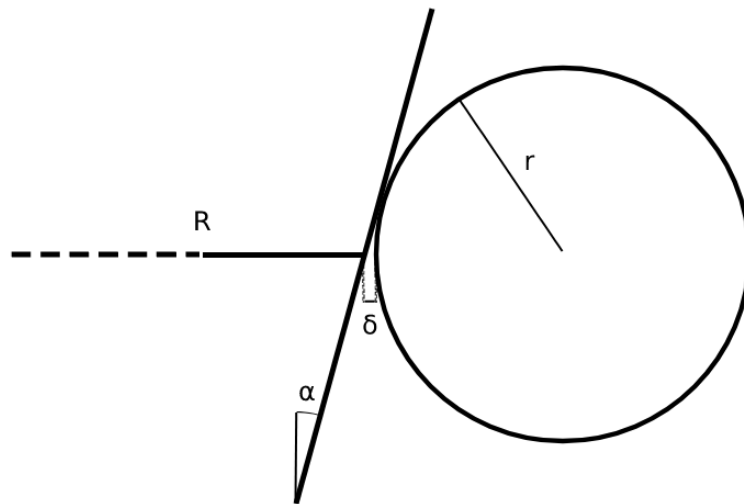


Figure 3.9: Illustration of the deviation between guide curve radius and roller position.

3.5.5 Final Curve Functions

Combining all the substitutions and corrections detailed in this section, we end up with two functions defining two sections of the guides: one controlling the steering angle of the inner wheel, and one controlling the steering angle of the outer wheel. Using the two sided concept (3.4.2), both these sections are mirrored on the opposite side of the double-guide wheel, thus one side of the wheel drives the inner wheel as the opposite side drives the outer wheel. The direction the steering wheel is turned governs which section of each curve is active.

Of course, the guides in their final production needs an actual thickness, so both guide functions were copied and shifted 2 mm outwards/inwards, creating a 4 mm wide guide (minus the before mentioned correction function).

Figure 3.10 shows the curves. The complete parametric polar coordinate function that defines a1 is shown on the subsequent page (units are radians and mm). To get a2, the zero point of 57 is replaced by 53. To get b1 and b2, all the t 's except the one in the linear approximation of the curves derivative must be substituted by equation 3.4, and the linear approximation of the curves derivative must be swapped with the one for the outer wheel.

Written out in text format these become four very long parametric polar coordinate functions with countless brackets and many repeated sections. Managing these in Inventor was difficult, as the viewing window was too small to view more than one fifth of the functions at a time. As mentioned in 3.5.4, the reason the derivative functions were replaced by a linear approximation was to keep the functions from becoming even longer and less manageable. The complete radial components of the functions in text format as they are entered into Autodesk Inventor are seen on page 34.

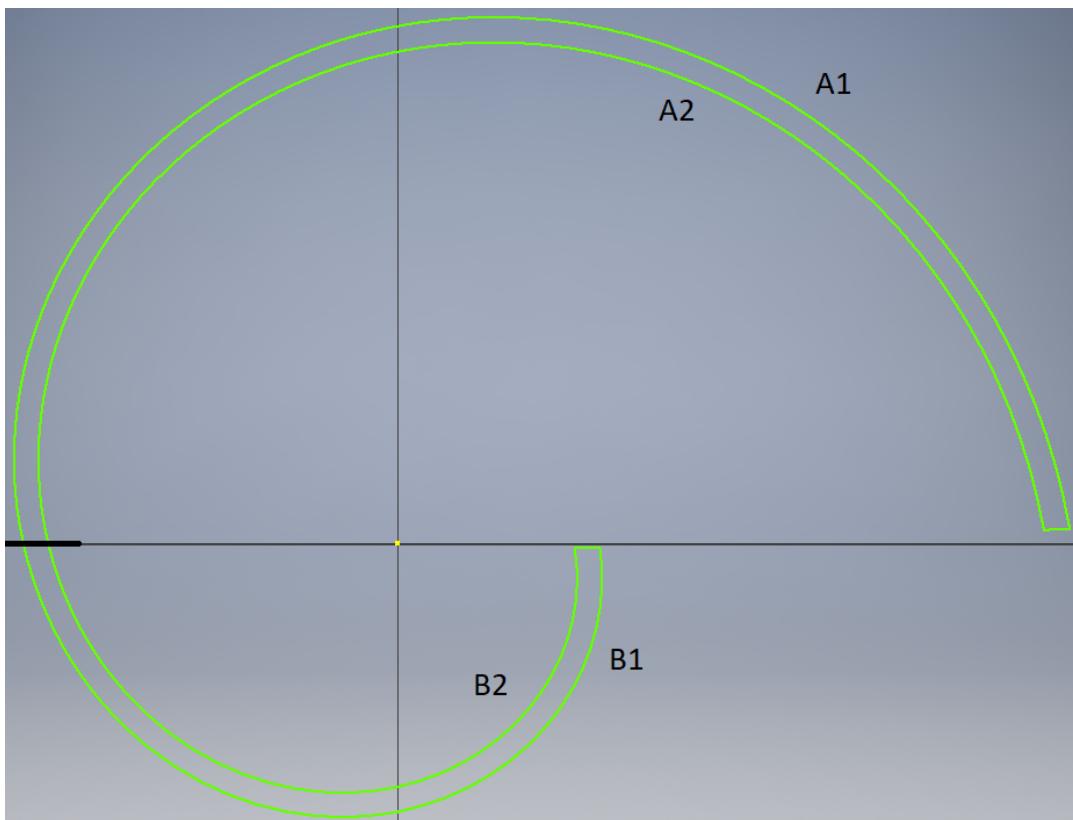


Figure 3.10: The four curves present on both sides of the DGW.

$$R_{a1} = 57 + 170 * \left[\frac{1 - \cos \left(\operatorname{asin} \left(\cos(0.5764) - \cos(0.5764 + t) \right) * 119.27 / 170 \right) \right] - 119.27 * (\sin(0.5764 + t) - \sin(0.5764)) \dots$$

$$- \frac{4}{\cos \left[\operatorname{atan} \left(\frac{(45*t - 100.3) / 7.8}{57 + 170 * \left[1 - \cos \left(\operatorname{asin} \left(\cos(0.5764) - \cos(0.5764 + t) \right) * 119.27 / 170 \right) \right] - 119.27 * (\sin(0.5764 + t) - \sin(0.5764)) \dots} \right) \right]}$$

$$+ 4$$

$$\theta_{a1} = 7.8t$$

- a) $1 \text{ 57 mm} + 170 \text{ mm} * (1 \text{ ul} - \cos(\text{asin}(\cos(1 \text{ rad} * 0.5764 \text{ ul}) - \cos(1 \text{ rad} * 0.5764 \text{ ul} + 1 \text{ rad} * t))) * 119.27 / 170 \text{ ul})) - 119.27 \text{ mm} * (\sin(1 \text{ rad} * 0.5764 \text{ ul} + 1 \text{ rad} * t) - \sin(1 \text{ rad} * 0.5764 \text{ ul})) - 4 \text{ mm} / \cos(\text{atan}(\cos(45 * t - 100, 3) / 7.8) / ((57 + 170 * (1 \text{ ul} - \cos(\text{asin}(\cos(1 \text{ rad} * 0.5764 \text{ ul}) - \cos(1 \text{ rad} * 0.5764 \text{ ul} + 1 \text{ rad} * t))) * 119.27 / 170 \text{ ul}))) - 119.27 * (\sin(1 \text{ rad} * 0.5764 \text{ ul} + 1 \text{ rad} * t) - \sin(1 \text{ rad} * 0.5764 \text{ ul}))) + 4 \text{ mm}$
- 2 $53 \text{ mm} + 170 \text{ mm} * (1 \text{ ul} - \cos(\text{asin}(\cos(1 \text{ rad} * 0.5764 \text{ ul}) - \cos(1 \text{ rad} * 0.5764 \text{ ul} + 1 \text{ rad} * t))) * 119.27 / 170 \text{ ul})) - 119.27 \text{ mm} * (\sin(1 \text{ rad} * 0.5764 \text{ ul} + 1 \text{ rad} * t) - \sin(1 \text{ rad} * 0.5764 \text{ ul})) + 4 \text{ mm} / \cos(\text{atan}(\cos(45 * t - 100, 3) / 7.8) / ((53 + 170 * (1 \text{ ul} - \cos(\text{asin}(\cos(1 \text{ rad} * 0.5764 \text{ ul}) - \cos(1 \text{ rad} * 0.5764 \text{ ul} + 1 \text{ rad} * t))) * 119.27 / 170 \text{ ul}))) - 119.27 * (\sin(1 \text{ rad} * 0.5764 \text{ ul} + 1 \text{ rad} * t) - \sin(1 \text{ rad} * 0.5764 \text{ ul}))) - 4 \text{ mm}$
- b) $1 \text{ 57 mm} + 170 \text{ mm} * (1 \text{ ul} - \cos(\text{asin}(\cos(1 \text{ rad} * 0.5764 \text{ ul}) - \cos(1 \text{ rad} * 0.5764 \text{ ul} + \text{atan}(1745 \text{ mm} / (1745 \text{ mm} / \tan(1 \text{ rad} * t) + 1115 \text{ mm})))) * 119.27 / 170 \text{ ul})) - 119.27 \text{ mm} * (\sin(1 \text{ rad} * 0.5764 \text{ ul} + \text{atan}(1745 \text{ mm} / (1745 \text{ mm} / \tan(1 \text{ rad} * t) + 1115 \text{ mm})))) - \sin(1 \text{ rad} * 0.5764 \text{ ul})) - 4 \text{ mm} / \cos(\text{atan}(\cos(148, 5 * t - 100, 3) / 7.8) / ((57 + 170 * (1 \text{ ul} - \cos(\text{asin}(\cos(1 \text{ rad} * 0.5764 \text{ ul}) - \cos(1 \text{ rad} * 0.5764 \text{ ul} + \text{atan}(1745 \text{ mm} / (1745 \text{ mm} / \tan(1 \text{ rad} * t) + 1115 \text{ mm})))) * 119.27 / 170 \text{ ul}))) - 119.27 * (\sin(1 \text{ rad} * 0.5764 \text{ ul} + \text{atan}(1745 \text{ mm} / (1745 \text{ mm} / \tan(1 \text{ rad} * t) + 1115 \text{ mm})))) - \sin(1 \text{ rad} * 0.5764 \text{ ul}))) + 4 \text{ mm}$
- 2 $53 \text{ mm} + 170 \text{ mm} * (1 \text{ ul} - \cos(\text{asin}(\cos(1 \text{ rad} * 0.5764 \text{ ul}) - \cos(1 \text{ rad} * 0.5764 \text{ ul} + \text{atan}(1745 \text{ mm} / (1745 \text{ mm} / \tan(1 \text{ rad} * t) + 1115 \text{ mm})))) * 119.27 / 170 \text{ ul})) - 119.27 \text{ mm} * (\sin(1 \text{ rad} * 0.5764 \text{ ul} + \text{atan}(1745 \text{ mm} / (1745 \text{ mm} / \tan(1 \text{ rad} * t) + 1115 \text{ mm})))) - \sin(1 \text{ rad} * 0.5764 \text{ ul})) + 4 \text{ mm} / \cos(\text{atan}(\cos(148, 5 * t - 100, 3) / 7.8) / ((53 + 170 * (1 \text{ ul} - \cos(\text{asin}(\cos(1 \text{ rad} * 0.5764 \text{ ul}) - \cos(1 \text{ rad} * 0.5764 \text{ ul} + \text{atan}(1745 \text{ mm} / (1745 \text{ mm} / \tan(1 \text{ rad} * t) + 1115 \text{ mm})))) * 119.27 / 170 \text{ ul}))) - 119.27 * (\sin(1 \text{ rad} * 0.5764 \text{ ul} + \text{atan}(1745 \text{ mm} / (1745 \text{ mm} / \tan(1 \text{ rad} * t) + 1115 \text{ mm})))) - \sin(1 \text{ rad} * 0.5764 \text{ ul}))) - 4 \text{ mm}$

3.6 System Design

3.6.1 Steering System Placement

As production had progressed on the FF19 chassis and internal structure, it was easier to see where the steering system could fit. The area in front of the dashboard had sufficient space and would allow the system to be mounted in between the wheels. This was an advantage as it meant the system could drive the steering knuckle directly through tie-rods, not having to use hydraulics or wires. The disadvantage of this mounting position was thought to be the risk of the driver kicking and damaging the steering system when entering or exiting the vehicle, as the system would be suspended above the drivers legs. Still, the superior simplicity of using this mounting position resulted in it being chosen.

Another benefit of this position was that the dashboard offered both the necessary space and rigidity for mounting autonomous actuators, in addition to having close proximity to other electronic mounts and systems. At the point at which the steering system placement was selected it had already been decided that FF would not compete in the SEM19 Autonomous competition, as it was moved to a separate event in the Netherlands in May. The team had neither the time nor resources to attend this separate event. Still, the prospect of competing in 2020 led to the regard for autonomous operation to be maintained.

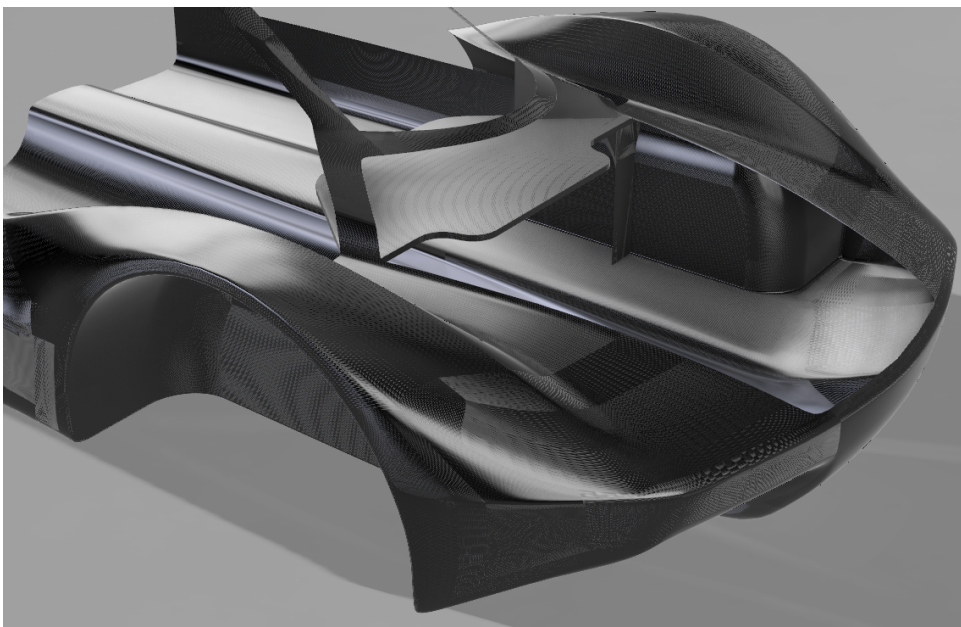


Figure 3.11: Render of the front of the chassis, showing the available space in front of the dashboard.

The selected position mounts the steering system in front of the front axle, meaning the direction of steering relative to the direction the tie-rods move is reversed. If a rack and pinion system was to be mounted in this position

the steering arms would need to point away from the vehicle to achieve Ackermann geometry. Utilising the double-guide wheel meant that the direction of travel of the tie-rods relative to the rotation of the steering column could be altered freely, and so this was a non-issue.

3.6.2 Material Selection and Dimensioning

Material Selection

The criterion for selecting a material to produce the double-guide wheel were as follows:

- Be available in suitable sizes and thicknesses. Preferably a plate or flat bar so that large amounts of material removal is not necessary to manufacture a flat part such as the double-guide wheel.
- Be low in mass density, and relatively strong compared to weight.
- Do not be costly.
- Be available for quick purchase and delivery.

After browsing the selection of several local distributors, a 150 mm wide and 15 mm thick flat bar of 6082-T6 aluminium was purchased. This had the highest yield stress of the available aluminium alloys in similar dimensions, could be delivered the same week, and cost the team only 53 NOK per kg. The supplier guarantees a tensile yield strength of 255 MPa, and an elastic modulus of 70 GPa[15, pg.98].

High Speed Turning

We'll now assume that there is a self-centring torque applied to the wheels during turning, as the result of a caster angle built into the suspension system. The transverse loads on the wheels during turns is based off of analysis made in the pre-master thesis leading up to this master thesis.[16, pg.29] Team member Christian André Pettersen is in charge of driving strategy during SEM19. According to his analysis, the sharpest turn during the race is likely to be a 13.5 m radius turn, performed at 25 km/h. Using the analysis for worst case transverse load on a wheel in the pre-master thesis this results in a 211 N transverse load on the outer front wheel.

Assuming a wheel diameter of 580 mm and a positive caster angle of up to 5°, the steering axis intersects the ground ahead of the contact patch between the tyre and the road. Meaning the transverse loads on the tyre creates a moment arm about the steering axis of up to $580 \text{ mm} / 2 * \sin(5^\circ) = 15 \text{ mm}$. With a transverse load of 211 N, this causes a torque of $211 \text{ N} * 0.015 \text{ m} = 3.2 \text{ Nm}$, which is absorbed by the steering arm. With a steering arm length of e.g. 80 mm, the load on the tie-rod or piston driving the steering arm

is $3.2 \text{ Nm}/0.08 \text{ m} = 40 \text{ N}$. This load carries through to the guides of the double-guide wheel.

Standstill Turning

A simple experiment was performed to see whether the Resistance to turning during standstill could be a dimensioning factor. MTP masters student Markus Lid sat in the FF19 car to provide the correct weight distribution (70 kg driver including ballast if necessary is required according to SEM rules[1]). The caster was set to 0° while the wheels were turned by pulling each tie-rod individually with a luggage weight. The weight reads the load as the equivalent of a mass in kg under standard gravity. The test was performed three times, with the highest reading showing 4.6 kg, the equivalent of 45 N.

It is seen from this that the maximal loads from standstill turning are marginally higher than those from high-speed turning. However, the calculated loads from high speed turning does not include any resistance in the system itself, or other centring factors apart from caster.

Simulation

A FEM analysis was performed on a CAD-model of a version of the double guide wheel in which the guides were 4 mm thick and the wheel itself 2 mm thick. The wheel was constrained at the centre and a point load of 45 N was placed at the most exposed point of the part. The analysis was performed in Fusion 360, using automatic meshing and default analysis settings. The results showed a maximum stress level of 105.8 MPa directly at the contact area. However the highest Von Mises stresses away from the immediate vicinity of the point load were approximately 40 MPa, only 16% of the yield stress of Alu 6082-T6[15][pg.98]. When applying point loads in FEM analysis, contact stresses are often inaccurately simulated, as mathematical singularities occur when a load is placed on a single node.[17][chpt.9] With an elastic modulus of 70 GPa, the maximal resulting displacement was found to be 0.10 mm, located at the point of load application.

Contact Stress

Let's also consider the analytically determined contact stress at the interface between the rollers and the guides with the basis of Hertz' theory of non-adhesive contact.[18, pg.187] When a cylinder is pressed against a plane they

deform to create a rectangular contact patch, in which there is pressure between the two bodies. The maximal contact pressure between a cylinder and a plane is given by:

$$p_{max} = 0.418\sqrt{\frac{QE}{lr}} \quad (3.8)$$

in which Q is the applied load, E is the elastic modulus of both the materials and l and r is the length and radius of the cylinder. The Poisson's ratio is assumed to be 0.3. Underneath the contact patch the pressure causes internal stress. The largest shear stress occurs at a depth equal to 40% of the contact patch width, and has a magnitude of $0.3p_{max}$. According to the Tresca yield criterion, to avoid material yielding the shear stress should not exceed 50% of the materials yield strength ($R_{p0.2}$)[19]. Thus to avoid yield we get:

$$p_{max} = 0.418\sqrt{\frac{QE}{lr}} = \frac{\tau_{max}}{0.3} = \frac{R_{p0.2}/2}{0.3} \quad (3.9)$$

Assuming roller radius and length of 4 by 7 mm and yield strength and elastic modulus of 255 MPa and 70 GPa (Al 6082-T6 [15, pg.98]), we solve for the maximum permitted load, Q :

$$Q_{max} = \frac{lr}{E} \left(\frac{R_{p0.2}/2}{0.3 * 0.418} \right)^2 = 414N \quad (3.10)$$

Considering the loads discussed in this section, material yield as a result of contact stress is not a dimensioning factor.

Decision

Based on the analysis and performed tests, the guides and guide wheel could easily have been reduced in thickness compared to that in the CAD model used in the FEM analysis, if the before mentioned aluminium alloy mentioned is used to construct the part and material yield is the only concern. However, two other concerns were present: the desire to keep displacement low, so as not to affect steering geometry; and the fear that the part might be damaged from other causes than normal use if made too fragile. After attempting to cut up small pieces of the material in question and seeing how easily they were damaged by bending, dropping, stepping on and scratching a decision was made to stick with the 4 mm thick guides, and 2 mm thick wheel. This might have been a drastic over-dimensioning relative to operating loads, however the trade-off from reducing the dimensions were small. Reducing the thickness of the guide to just 2 mm would still only have saved 26 grams of weight.



Figure 3.12: The double-guide wheel straight out of the CNC milling centre.

3.7 Steering System Production

3.7.1 Double-guide Wheel Production

Four holes were drilled through a stock piece of alu 6082-t6 at known relative positions. Similar holes were drilled in a faced sacrificial plate in the CNC milling centre, after which the stock was mounted to the sacrificial plate by screws through the holes. The double-guide wheels features were milled by a series of pocket machining and contour machining processes. The stock was flipped over, and the same processes were performed on the opposite side, to create the two-sided nature of the component. The CAM process was aided by Børge Holen, section engineer at Verkstedteknisk laboratorie. Lastly, the part was separated from the stock, while leaving a series of tabs to be removed by hand.

3.7.2 Roller Production

The roller groups consisted of two aluminium rollers, two steel pins and two bearings each, all mounted to a block of aluminium. The smallest available bearings were used, needle roller bearings with ID 3 mm, OD 5 mm and length 7 mm. Thus the pins needed to be 3 mm in diameter. The rollers outer diameter was set at 8 mm, as this was the measurement used when determining the curve correction function (3.5.4). The parts were turned in a manual lathe.



Figure 3.13: The rollers, pins and bearings.

3.7.3 Mounts

The double-guide wheel was mounted to the carbon fibre steering column from FF18 by the use of Araldite 2048 glue. The shaft was mounted to the dashboard through two PLA 3d-printed mounting brackets. The pistons driven by the wheel needed to be mounted to each side of the DGW, and align with the tie-rods driving the steering arms of each wheel. This was solved by the use of an assembly of aluminium flat bars and CFRP tubes, held together by a 3d-printed assembly. The system consists of four main components:

- The aluminium flat bars that hold the roller groups. One of these is mounted in front of the front face of the DGW, the opposite one is mounted behind the rear face of the DGW, for the rollers to reach the relevant guides. Alu flat bar was used to prevent rotation, as transverse load is applied to the rollers. Other solutions to this problem were tested, but not found effective.
- The CFRP tubes that translate linear motion between the aluminium flat bars and the tie-rods. These are aligned with the steering arms of each wheel and the centre of the DGW.
- Offsetters. These connect the two aforementioned components, translating linear motion from one axis to another.
- Brackets. These hold all the pieces in place and mounts them to the dashboard.

All parts except the mentioned aluminium and CFRP tubes were made from 3d-printed PLA or PETG. The main justification for this was the ease of manufacturing, especially considering that the dashboard had been sloppily mounted by hand and was not level. To determine the correct relative mounting positions to the dashboard, a wooden plate was CNC milled to fit inside the car's wheel wells, with holes placed so that the wheel well centre point,

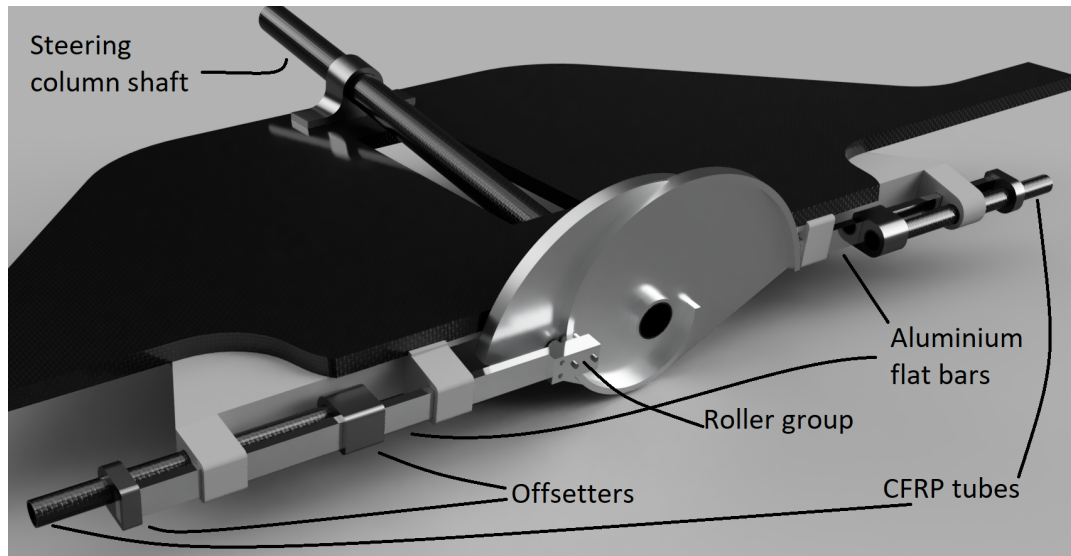


Figure 3.14: Annotated render of the steering system assembly.
The CFRP tubes further connect to the tie rods at each end.

vertical and horizontal axes, and the point at which the axis between the steering arms and the wheel well wall intersects could be marked onto the wheel well. Small holes were drilled through the latter, and a string was pulled taut between the two holes. This was used to measure the slope of the dashboard relative to the string, and the vertical and longitudinal distances at different points.

Several versions of the mounts had to be made before a good, level fit was achieved. The brackets were placed to minimise free length of any piston or tube. The CFRP tubes and alu flat bars slide freely inside holes in the mounts. These holes were intentionally made slightly too tight, and then filed and sanded to ensure a good fit with low friction.

3.7.4 Reproduction

Testing quickly unveiled two issues:

- The machining of the tabs in the DGW had caused indentations in the guide itself, reducing the smoothness of operation (3.15).
- There was at least one instance at which roller pins caught on to the edge beneath the guides, at the point where the guides went from not having material underneath them to having it. This caused the steering to "lock up", and caused two of the roller pins to bend.

Three measures were taken to prevent these issues. Firstly, the roller groups were spaced slightly further away from the DGW to avoid sliding against the wheel and catching on to features. Secondly, new bearings were purchased with a 4 mm ID and 7 mm OD. This enabled remaking the roller pins and rollers, so that the roller pins had an increased diameter from 3 to 4 mm,



Figure 3.15: The indentations caused by the machining of the tabs. The edge in the lower right corner of the photo is where the roller pins caught on.

more than doubling their bending strength. And thirdly, the DGW was remachined, this time adding a small shoulder along the guide. This ensured that there were no features for the pins to catch onto, and moved the tabs away from the guides, so that the machining of the tabs would not cause harm to the guides.

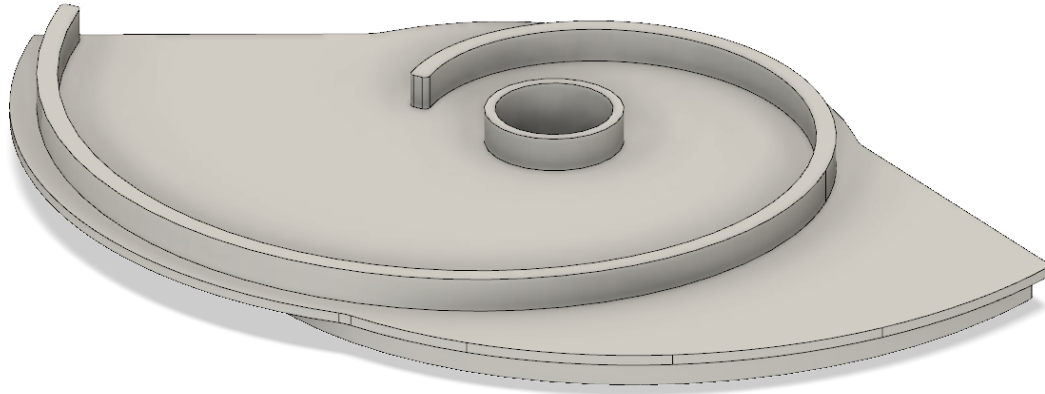


Figure 3.16: The shoulder is seen alongside the guide on the left side of the render and behind the guide in the top right side of the render.

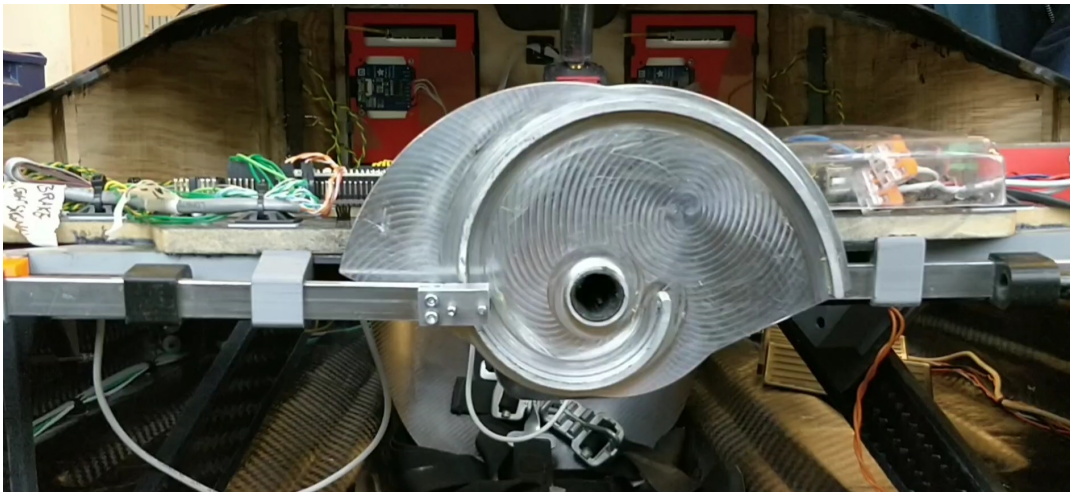


Figure 3.17: The finished steering system installed in FF19. [Click the figure or caption to see an animated version \(large file\)](#)

Chapter 4

Suspension System Development

4.1 Room for Improvement

Figure 4.3 displays the FF18 suspension and steering knuckle assembly, as designed by previous team members. The system consists of two pairs of suspension arms. The lower pair of arms is connected to an air dampener that absorbs the vertical loads on the system and allows some displacement during impact. At the end of each pair of arms is an angle joint that connects the arms to each end of the steering knuckle. The steering knuckle features a bearing housing in the centre and has mounts to hold a brake caliper on one side and a steering arm on the other. The spindle consists of an axle, a brake disc mounting plate, and a wheel hub mount – all in one piece.

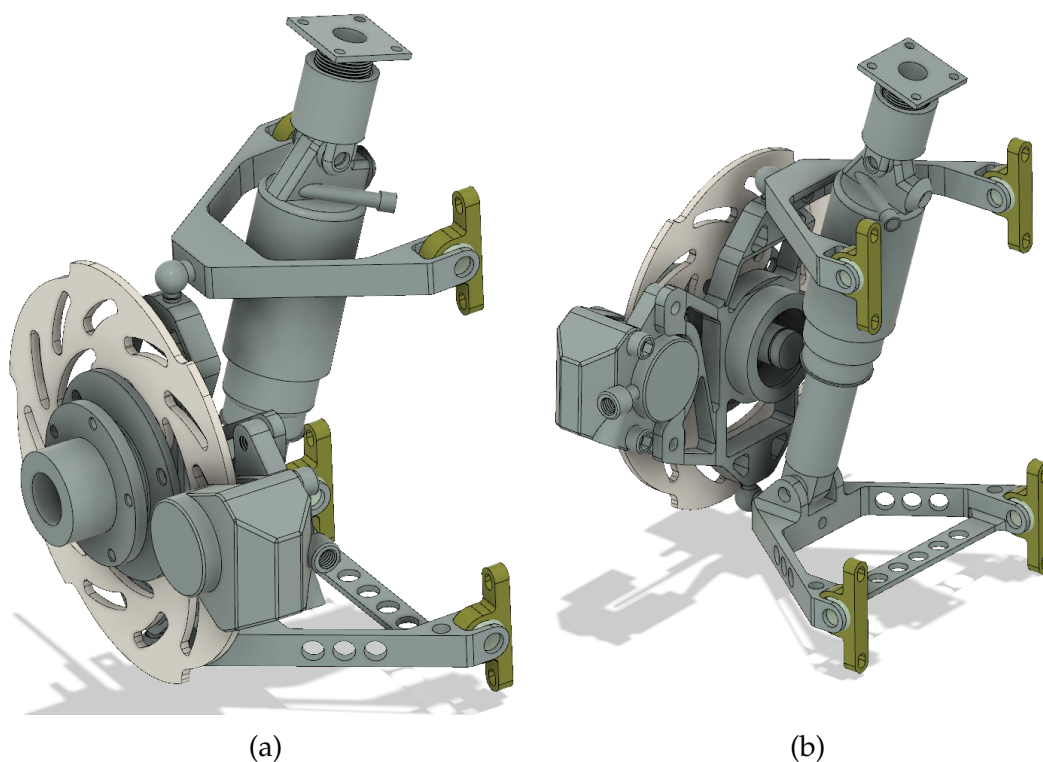


Figure 4.1: Old suspension and steering knuckle assembly

In a project like DNV GL Fuel Fighter there is not capacity nor sufficient funding to redesign and remake every component every year. Therefore, before deciding which parts need to be remade there is an evaluation of the necessity of swapping the existing part. In this evaluation the team considers whether the existing part is still functional in itself, whether it works well with the chassis and other new surrounding components, and whether there is reason to believe substantial improvement in performance is within reach if choosing to remake the component. During these evaluations it was discovered that the old suspension system in itself would not be able to fit the new chassis. Consequently the system was studied further to evaluate what might be improved upon – were a new system to be made. This section looks into the different areas in which it was discovered that improvement could be made. The evaluation is based on inspection of the parts, discussions between the project manager Eirik Furuholmen, brake system engineer Jennifer Nguyen, and the author, in addition to experiences made by last years team during the Shell Eco-marathon 2018. Some of these experiences are undocumented, and have been passed on orally to the author by former team members.

4.1.1 Bearings

The origin of the bearings was not known or documented within the team, thus any evaluation of them is based on inspection. The FF18 steering knuckle holds a single bearing, OD 47 mm, ID 20 mm and width 20 mm. This raised immediate concerns, as the axle is subjected to bending moments, which can not easily be absorbed by a single bearing. However, due to its large width one might assume that the bearing is most likely a double groove bearing. The fact that the current system has been functional is in itself evidence that the bearing has some capability of absorbing a bending moment. However, simply applying a load by hand while turning the spindle and observing showed that some degree of misalignment occurs when bending moment is applied.

After SEM18, scratch marks were discovered on the inside of one of the front rims. It was hypothesised by the FF18 team that these were made by the brake calipers rubbing against the rim as the system deformed under high load. Misalignment of the axle could have contributed to this. In addition to the concern of bending moment absorption, the bearings in them selves did not feel fast. Friction measurements were not made, however after initiating spin of the axle by hand it came to a stop quite quickly.

If a new steering knuckle was to be made it should therefore be made with bearings with a high capability of absorbing a bending moment, in addition to the radial and axial loads. An example of such a bearing system is a pair of opposite facing angular-contact ball bearings.[25] With a pair of bearings, the distance between them can be altered, giving a more stable platform than the 20 mm wide double groove bearing in the FF18 system.

4.1.2 Sweep Radius

As discussed in 2.4.2, a large sweep radius increases driver effort and causes toe when driving. The FF18 system was originally designed to be used with a set of aluminium rims, until these were swapped with a set made from carbon fibre composite. The newer set of rims allows the steering knuckle to be mounted deeper into the rim. The steering axis inclination might therefore no longer provide optimal sweep radius reduction.

4.1.3 Shock Absorber

During SEM18 many adjustments were made during test runs in an effort to maximise the cars performance. One of these adjustments was to increase the dampening stiffness of the front suspension. According to the FF18 team, this had a great positive impact on performance, although not on driver comfort. The team ended up bringing the front suspension to a full lock-out during the competition.

Increasing suspension stiffness has obvious negative side-effects, like increasing vibrations in the car and the load on the suspension when driving across an uneven surface. However, as the FF18 team ended up locking out the front suspension fully, the question arose whether it was worth it to keep the shock absorber in place at all. Removing the shock absorber would allow for substantial weight savings. Having no shock absorber would also remove any interference of steering caused by the vertical wandering of the suspension system.

4.1.4 Brakes

The front brakes of the vehicle relies on a pair of brake discs, weighing approximately 748 *grams* per disc. The team is also in possession of another pair of discs that meet SEM requirements, weighing only 437 *grams* per disc. However, the lighter set of brake discs does not fit the FF18 steering knuckle. Remaking the steering knuckle could therefore potentially allow the use of the lighter discs.

As the brake discs rotate with the wheels, they require kinetic energy not just to achieve translation movement, but also spin. This means that reducing the weight of the brake discs by one gram has a higher effect on efficiency than reducing the weight of a static component by the same amount. Reducing the weight of rotating components should therefore be of higher priority than reducing the weight of static components.

4.2 Steering Knuckle Design

4.2.1 Material Savings

At the point in time at which the steering knuckles were produced, the teams budget was close to be blown. Therefore it was made a priority to not purchase new materials and parts unless absolutely necessary, but rather use left-overs from earlier builds.

Among available materials was a long flat bar of Alu 6082-t6, 150 mm wide, 15 mm thick, which was left-over from the steering system production. Additionally, several pieces of aluminium 7075-t6 were available, in the shape of different sized pieces of 30 and 50 mm plates. The rod-ends and angle joints used to mount the FF18 steering knuckle to its suspension were also available, as well as the brackets used to mount the FF18 suspension to the car's wheel wells. Two sets of carbon fibre tubes were available., approximately 2.5 meters of OD 12 mm tubing, and 0.7 meters of OD 20 mm tubing. All with a wall thickness of 1 mm.

4.2.2 Zero Sweep Radius Design

Inspection of the carbon fiber rims showed that the rim wall was so close to the front surface of the rim that the steering axis could in theory pass through the centre of the rim. Utilising this would enable the achievement of zero sweep radius, without applying any steering axis inclination or camber. This could potentially resolve several issues:

- No rising of the front of the car while turning.
- No difficult static/dynamic toe corrections having to be made.
- Fewer factors interfering with steering geometry, increasing confidence in steering angles.

As can be seen in figure 4.2, there is a very limited amount of space between the centre of the rim, and the rim wall. In order to fit the steering axis that deeply into the rim, the brake disk and caliper would have to be on the back

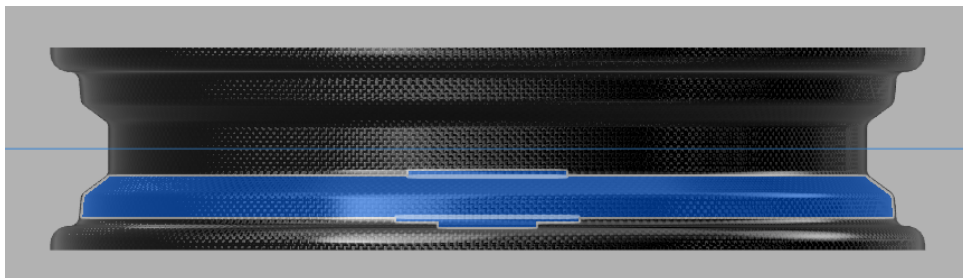


Figure 4.2: Space inside the carbon fibre rim.

side (facing the car) of the steering knuckle. Such a design would also demand a lengthening of the steering knuckle compared to the FF18 version, in order for the suspension to reach around the brake disc.

4.2.3 Three Layer Concept

In order to fit the brake disc and caliper on the back side of the steering knuckle it needed to be thicker than the FF18 steering knuckle. Machining the entire knuckle from one block of material would leave a large portion of the space in between the two bearings as a bulk of solid material, assuming a 3-axis CNC mill is used with end-mill tooling (the one available at Verkstedtekniske laboratorier). Additionally, a lot of material would have to be removed, as the thickness of the stock would be defined by the thickest section of the knuckle. In stead, the knuckle was designed in three layers that could be machined from the 15 mm thick alu 6082-t6 flat iron mentioned in 4.2.1. The front layer holds the first bearing and the joints connecting the knuckle to the rest of the suspension. The middle layer holds the brake caliper mounts,

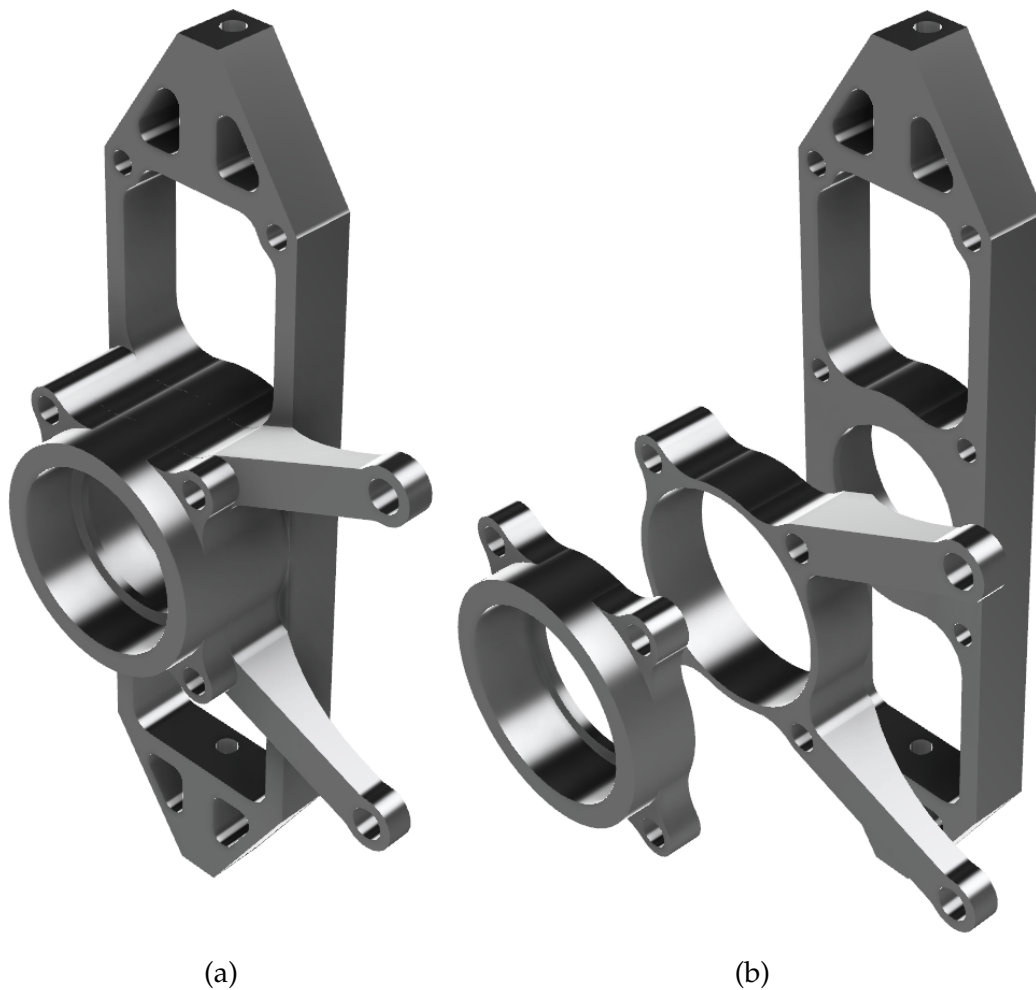


Figure 4.3: Three layer steering knuckle design.

and acts as a spacer between the two bearings. The middle layer is mostly hollow, which is the advantage of the three layer design, as this section would be the bulk of solid material left between the two bearings if the knuckle was machined from a single piece of stock. The back layer holds the second bearing. The thicknesses of the layers were 14 mm each, and was selected in order to leave 2 mm clearance between the knuckle and the brake calipers, and the rim wall. The three layers were designed to be held together by four M6 screws.

4.2.4 Spindle

The spindle going through the steering knuckle had two requirements: the front end needed to fit the hub of the teams carbon fibre rims and the rear end needed to fit the new brake discs mentioned in 4.1.4. In the FF18 steering knuckle the hub mount, brake disc mount, and axle were all turned from a single piece of stock. However, as the new design has components on both sides of the knuckle, it needed to be able to be disassembled. The spindle was therefore designed in three separate pieces. The hub mount was designed to be mounted to the axle by a pin going through both radially, while the brake disc mount was designed to fit on a hexagonal end section of the axle. This way, axial location and torque transfer became in-dependant, and the brake disc mount could be fit on the axle with a slight pre-load against the bearings, ensuring a tight fit. A screw inside the axle and disc presses the brake disc mount against the rear bearing. All spindle components would be machined from the alu 7075-t6 material available.

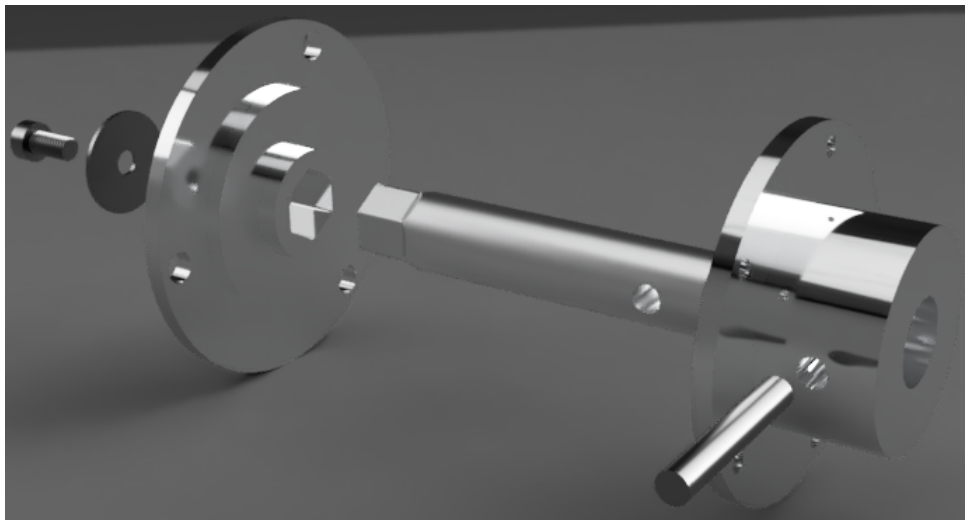


Figure 4.4: Exploded view of spindle assembly.

4.3 Suspension Arms

4.3.1 Carbon Fibre Tube Strength Test

A set of carbon fibre tubes mentioned in 4.2.1 were available in the teams inventory, however there was no data on the mechanical properties of these tubes. A simple test was performed in order to determine the bending strength and fracture stress of the material. A tube was placed between the edges of two tables, and a 5.1 kg metal bucket was hanged from the centre of the tube. Weights were added to the bucket by increments of 2.5 kg until fracture. The free length of the tested specimen was 226 mm, the inner and outer radius of the tube was 5 and 6 mm. Brittle fracture occurred at 62.6 kg, whilst 60.1 kg did not brake the tube.

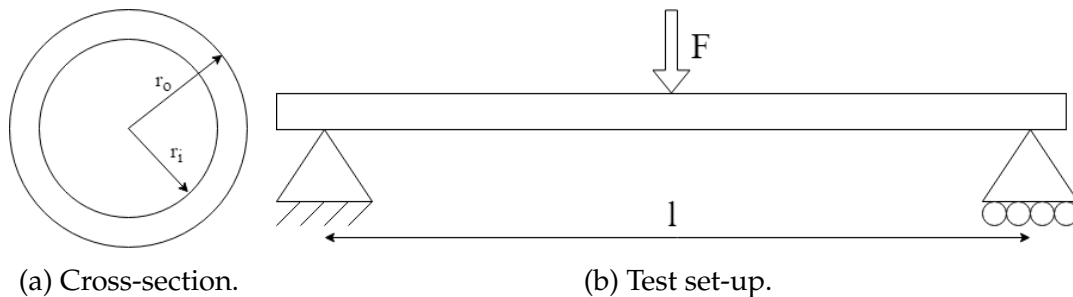


Figure 4.5

The maximum bending moment is given by:

$$M_{max} = F/2 * l * 2 [19] \quad (4.1)$$

and the maximum stress in the rod is given by:

$$\sigma_{max} = \frac{M_{max}}{\pi/4 * (r_o^4 - r_i^4)} * r_o [19] \quad (4.2)$$

Assuming standard gravity, the test showed that the bending strength and fracture stress of the rod lies in the ranges 33.3 Nm to 34.7 Nm and 379 MPa to 395 MPa.

In comparison, the FF17 suspension was made from alu 7075-t6, with a minimum cross-section of 5*16 mm. Assuming a yield strength of 503 MPa[26], this results in a minimum bending strength before yield of 33.5 Nm. Due to the low weight of the carbon fibre tubes, a suspension system was designed based on the use of these OD 12 mm tubes in-stead of aluminium, on the assumption that the tubes could provide sufficient strength.

4.3.2 Suspension Arm Layout

Based on the reasoning in 4.1.3, the system was designed without the use of a dampener. The lower suspension bars required a 28° inclination, in order to be mounted within the lower edge of the wheel well, and reach the lower end of the steering knuckle without colliding with the brake disc. At the top end of the steering knuckle, two bars were placed in a similar fashion as on the lower end, facing the opposite direction. Additionally, the larger OD 20 mm tubes were designed to be used at the top end of the knuckle, to absorb vertical loads in replacement of the dampener previously used. The spacing between the pairs of carbon fibre tubes was set to 60° , based off of previous studies performed by former team member Stéphanie Ear.

The design permitted the reuse of FF18 brackets and pins connecting the suspension to the wheel well, and joints connecting the suspension to the steering knuckle. To connect the tubes at the knuckle end, a connector made from aluminium with sides angled 30° outwards, and mounting holes at a 28° inclination was designed.

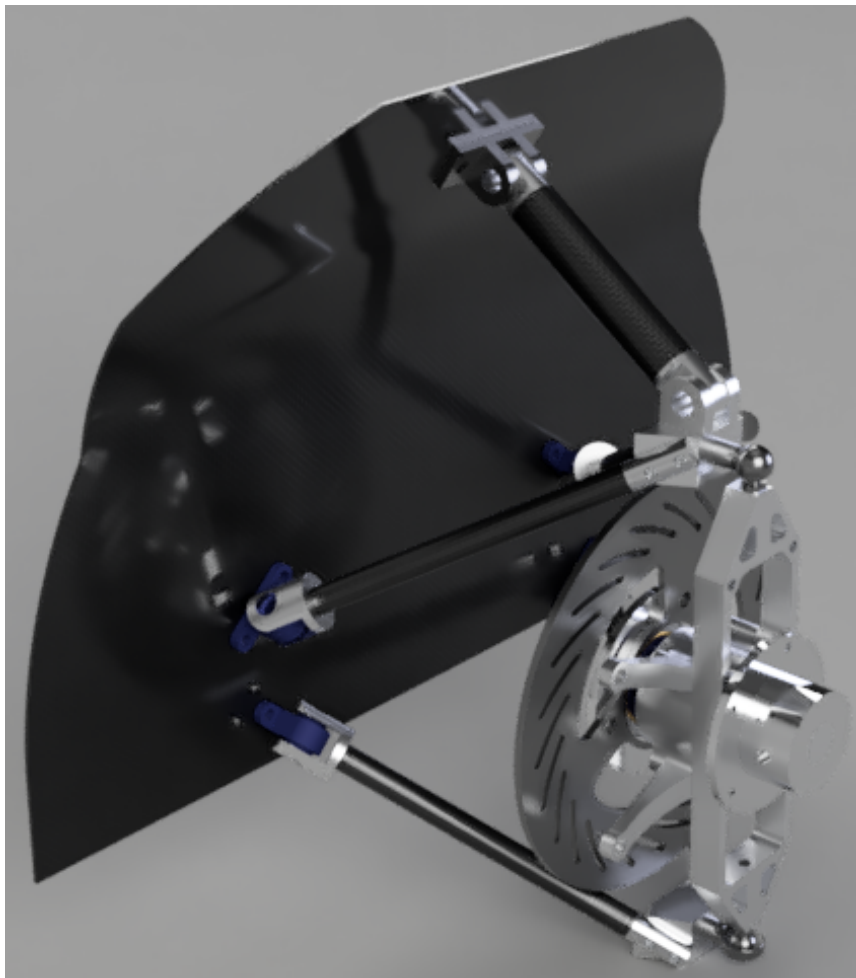


Figure 4.6: Render of suspension and steering knuckle assembly.

Since the design achieved zero sweep radius, the assumed demand for self-alignment was low. The caster angle was therefore set to 3° . It is the impression of the author that this is in the lower range of what might be seen in normal cars. Since FF19 has no power steering as opposed to normal cars, low driver effort was desirable, especially with regard to autonomous operation.

4.4 Dimensioning

4.4.1 Load Cases

Based on the continuation of work detailed in the pre-master thesis preceding this master thesis, three load cases for the front suspension have been developed. These represent the worst case loads that the suspension might be subjected to during use. When dimensioning parts for FF one must keep in mind that most parts have a very short service life, and fatigue is not of major concern. Parts should be designed to make it through testing and SEM, but limits must be pushed in terms of weight to have a chance of reaching the top of the podium.

High Speed Turning

The outer front wheel experiences the most severe loads, with 580 N vertical load, and 211 N transverse load. This load occurs during a realistic scenario of the tightest turn during SEM19

Maximum Power Braking

The front wheels both experience a 526 N vertical load and a 381 N longitudinal load. The longitudinal load creates a 110 Nm torque around the wheel axle, which is absorbed as a frictional load on the brake disc. This load case scenario represents the theoretical loads during maximum power braking on all four wheels. A true braking scenario would likely not be able to produce loads quite as high, due to imperfect balancing of the brake system.

Road Bump

The front wheels are subjected to a 2000 N vertical load. This load case represents driving over a bump at high speed, a scenario that should be avoided, but still one that is realistic enough to be taken into account during dimensioning.

4.4.2 Steering Knuckle

Axle

While the FF18 knuckle used a 20 mm axle, it was desired to reduce this dimension to 17 mm, equalling one step-down in bearing size. Reducing the diameter of the axle by just 3 mm, meant smaller and lighter bearings, and the bearing housing in the knuckle itself could be smaller and lighter as well.

Most of the FEM analysis that was performed during this master's project was done as simple linear studies in Fusion 360 or Inspire, using automatic meshing. These simple FEM methods are quick, and enabled the development of these systems within the given time frame. However, using simple methods increases the risk of inaccurate results. Safety factors were used to compensate for these inaccuracies. When analysing the stress response of the hexagonal connection between axle and brake disc mount under the maximal power braking load case, the linear analysis showed extremely high local stress concentrations.

To ensure that downsizing to a 17 mm axle was in fact a viable option, more in-depth analysis was performed. Fredrik Dahler and Nicholas Thuve were (at the time) masters students at the Department of Structural Engineering, and writing their master's thesis on dynamic FEM analysis of aluminium alloys. They assisted in setting up and running an explicit Abaqus study to test the axle/brake disc mount connection. The outer surface of the brake disc mount was constrained as the opposite end of the axle was subjected to the 110 Nm torque, ramped up over 0.05 seconds. The element size was set to 0.5 mm on the axle and 1 mm on the disk mount, C3D8R and C3D6R elements were used. All fillets and rounded edges were removed for optimal meshing.

The results showed peak stresses of 484 MPa as local stress concentrations on the axle, 96% of the yield stress of alu 7075-t6. In other words, the specimen in the study barely withstands yielding at the maximum theoretical braking loads. These results are skewed by three factors: the study only considers torsion, not the shear loads from the load application on the brake disc; the study assumes only hard edges, while the real part would have rounded edges, reducing stress concentration; aluminium is a highly ductile metal[27], therefore small areas of local yielding might not necessarily lead to component failure. Additionally, the maximum braking load-case was deemed unrealistically severe (this was later supported by braking tests that showed the system was only able to produce significantly lower braking loads). Taking these concerns into account, it was decided to keep the downsized 17 mm axle.

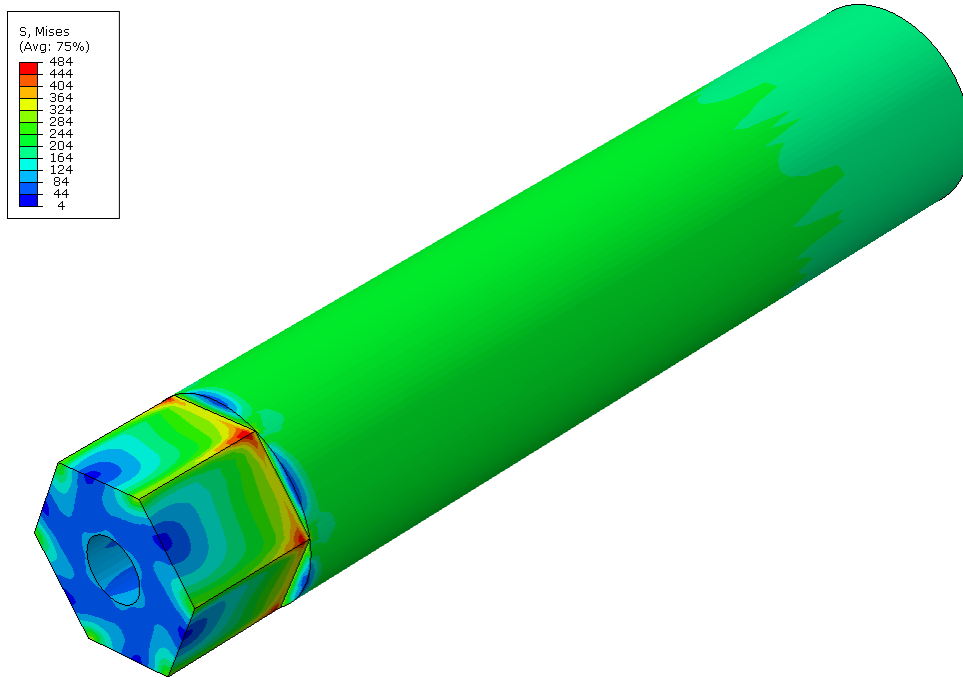


Figure 4.7: Resulting Von Mises stress distribution from Abaqus study

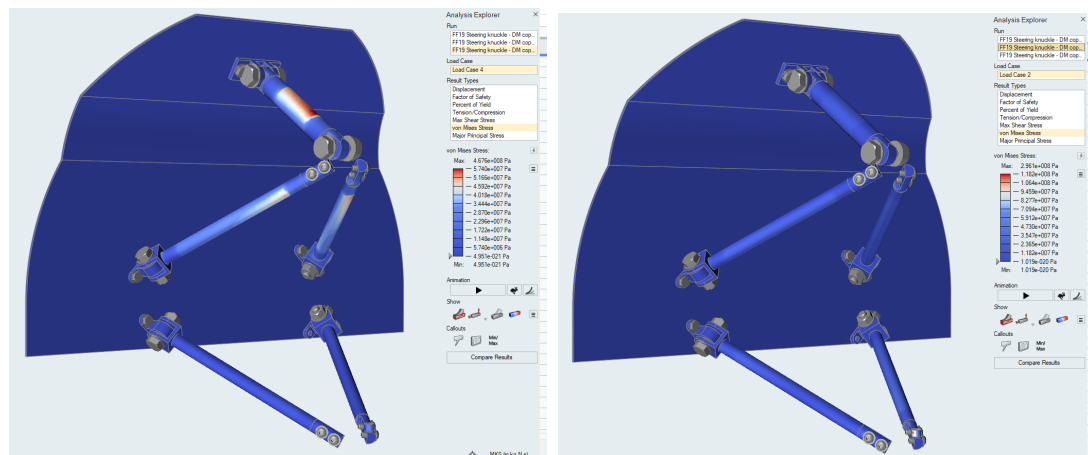
Geometric Layout

The general geometric design of the front layer of the steering knuckle was copied from the FF18 steering knuckle, as there was not sufficient time to pursue a new design concept. The structure was verified using topology optimisation studies in both Fusion 360 and Inspire, which suggested similar shapes. The thicknesses of each section was determined by starting with an overly sleek design, and increasing the thickness of each part of the design iteratively until a safety factor against yield of at least 3 was reached in every section, using Fusion 360 linear FEM analysis with automatic meshing.

4.4.3 Suspension Arms

An initial CAD design of all the connectors holding the CFRP suspension arms together was created as described in 4.3.2. This initial design was made to be as simple to machine as possible, without excessive weight or use of material. The intention was to strengthen weak points as they were discovered through FEM analysis. The entire setup was subjected to all three load-cases in Inspire FEM studies, and showed high safety factors in all sections, thus no strengthening modifications needed to be made. In these studies, linear static analysis was performed with automatic meshing. The CFRP tubes were represented by a constructed material, assumed to be homogeneous. This is not truly representative of CFRP, however, confidence in the design was maintained due to the high safety factors. The maximal Von-Mises stress found

in the CFRP rods was 57 MPa, given the bump load-case. The maximal Von-Mises stress found in the aluminium connectors was a local concentration of 118 MPa, given the maximum braking load-case. These are the two least realistic load cases, and still, safety factors of 6.5 and 4 are present assuming the results from 4.3.1, and Alu 7075-t6[26]. The analysis showed low deformations, with a maximum displacement of 1.6 mm during the bump load-case (a case which should not occur during normal operation).



(a) Suspension under bump load

(b) Suspension under braking load

Figure 4.8

4.5 Suspension System Production

4.5.1 Steering Knuckle Production

Production of the Three Layer Design

The steering knuckle CAD files were forwarded to Bjørn Martin Bendixen, section engineer at Valgrinda, who handled the production. The parts were made from the same Alu 6082-t6 stock as the steering DGW. Faced on one side, then flipped before features were CNC milled on the other side. The parts were deliberately designed so that all features could be machined with a 3-axis machine without unclamping the parts. The bearing housings were made to an H7 tolerance fit, tight enough for the bearings to stay firmly in place, but loose enough to allow assembly by hand. 7203 BE-2RZP angular contact bearings were provided by SKF, through a sponsorship agreement.

Spindle Production

The spindle parts were made from left-over Alu 7075-t6 from previous projects, in the form of 20, 30 and 50 mm plates. Square pieces were cut off using

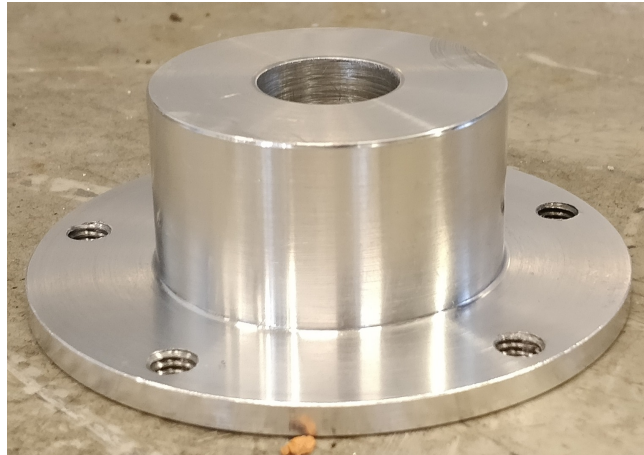


Figure 4.9: Finished hub mount.

a band saw and then turned with a heavy duty cutter to achieve a round shape. The hub mounts were turned and faced manually, then drilled, internally turned and finally broached with a 17 mm H7 broach. This was all done without removing the part from the lathe chuck, to ensure concentricity and co-axiality between the bore (holding the axle) and the outside of the mount (holding the wheel hub). The part was then flipped, so that the rear face of the hub mount could be faced. The wheel hub mounts to the spindle through five M6 screws. The hole locations were marked by clamping the hub mount inside the wheel's hub and punching the holes through the holes in the wheel hub. The holes were then drilled and tapped.

The axles were turned to fit tightly inside the hub mounts and bearings, whilst still being mountable by hand. One end of the axles were drilled and tapped to an M5 thread. The axles were then mounted to a horizontal rotary table on a manual mill. The hex connection between the axles and the brake disc mounts were milled by milling across the end of the axle while rotating it 60 degrees between each pass.

The brake disc mounts were CNC-milled, with Børge Holen once more assisting with the CAM process. The three mounting holes for the brake discs were first drilled and tapped by manual control of a separate mill. The stock was then mounted through these holes from underneath, to a sacrificial plate in the milling centre. All features were milled from one side. The hex bore was machined with decreasing step-over and tool sizes, moving down to a 2 mm end-mill. Thus, the corner radius of the hex bore is 1 mm.

The hub mounts and axles were mounted together by drilling through both, tapping one end of the bore, and installing a holding pin, made from an M6 screw with its head removed. Team members David Guerrero, Kristoffer Sydnes and Ole Andreas Wammer assisted in these operations.

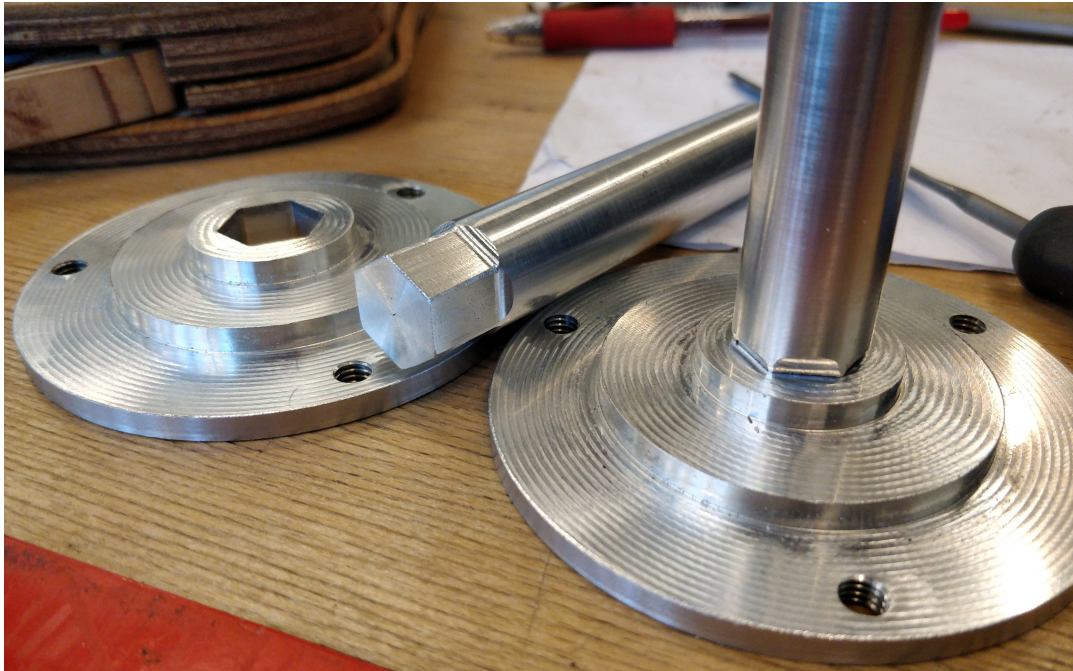


Figure 4.10: Test fitting of the axle and brake disc mount hex connection.

4.5.2 Suspension Arms Production

Tube-ends

Most of the brackets and pins mounting the suspension arms to the wheel well were reused from FF18, while the top mounting bracket was reused from an intermediate suspension system, designed and constructed by team member David Guerrero. Hinges that could fit inside the CFRP tubes and meet with these brackets were turned, milled and drilled from aluminium round stock off the shelf in Verkstedteknisk laboratorie, presumably alu 6086-t6. The section fitting inside the CFRP tubes were made to fit tightly, but had sections of reduced diameter to allow glue to sit. At the opposite end of the CFRP tubes, similar parts were made to secure the tubes to the connectors holding the top and bottom end of the steering knuckle. These parts also needed to be turned, milled and drilled. Tube-end production was assisted by team member Kristoffer Sydnes, and former team member Sarah Prescott.

Connectors

The connectors between the CFRP arms and the steering knuckle were milled from left-over Alu 7075-t6. The parts were clamped in the mill vice at 30 degrees, and faced off, before holes were drilled and tapped along a 28 degree line. The top connectors also included a mounting hole for the top CFRP tube, taking the vertical loads.



Figure 4.11: An overview of the main parts of the suspension system.

Assembly

The 12 mm CFRP tubes were cut to the correct lengths according to CAD files, and the tube-ends were glued in place with Araldite 2048. The tube-ends were secured to the connectors with M6 and M5 screws. The brackets were mounted to the wheel well, once more using the CNC-milled wooden template (3.7.3), placed inside the wheel well to locate the correct hole positions. The entire suspension was then mounted to the vehicle, excluding the 20 mm CFRP top tubes. These were cut slightly oversized according to the CAD model. They were then shortened iteratively, while measuring the angle of the mounted assembly, to ensure zero camber. Finally, the top tubes were also glued in place using Araldite 2048.



(a) Demonstration of the mounted suspension arms and steering knuckle front layer.

(b) Demonstration of the fully mounted suspension system, with brakes.

Figure 4.12: (The steering arm seen in these photos was a temporary version for testing purposes. A CNC-milled version was later made with help from Bjørn Martin Bendixen at Valgrinda.)

Chapter 5

Results

5.1 Steering System

5.1.1 Weight

The weight of the steering system was not a main concern during the development process. Instead, the focus was on determining whether a system could be made in which the designer had full control over the steering geometry. Yet, as with all other components in a vehicle such as FF19, weight should be taken into consideration when reviewing the final product.

The difference in weight between the FF18 and FF19 steering systems is a matter of perspective, or rather which features you choose to include in the measurements. The FF19 steering system is mounted to the dashboard, a feature which would none the less have to be present, were it or were it not for the steering system. The FF18 steering system was mounted to a central pillar, put in place for the sole purpose of supporting the steering system. This pillar is no longer in FF's possession, and therefore has to be excluded from the measurements. The different systems have steering columns of different length, but this is more a result of the different vehicle layouts than the steering systems themselves. Regardless, the columns are made from CFRP tubing, and make up a very small fraction of the weight, and so they have been excluded. Also excluded are the parts that are present in both systems, and therefore make no difference in weight. These are the rod-ends at each end of the tie-rods, and the ones connecting the steering system to the tie-rods.

Several parts were not weighed before they were glued together and to the dashboard, and can not be removed without destroying them. The weight of the FF19 steering system was therefore calculated based on CAD. The sliding alu flat bars and the DGW itself were assumed to have a density of 2710 kg/m^3 [28], while the alu 7075-t6 alu blocks holding the rollers were assumed to have a density of 2800 kg/m^3 [26]. The stainless steel rollers and roller pins were assumed to have a density of 8000 kg/m^3 ([29]), while the needle bearings were assumed to weigh 1 gram each. The CFRP tubes were

found to weigh 48 g/m, while the weight of the 3d-printed parts was calculated by the g-code generating software used to create them. This all resulted in a total weight of 638 grams.

The original 3d-printed bracket holding the FF18 rack and pinion system to the floor was no longer to be found at the time of the weighing. Its weight was assumed to be approximately equal to another version of it which had been used to fit the FF18 steering in FF19 for testing and fail-safe purposes. The weighing included the rack and pinion itself, a flexible joint used to change the angle of the FF18 steering column and the 3d-printed mount holding the rack and pinion. The total weight of these components is 560 grams.

When not including the central pillar and its mount used to hold the FF18 steering system, this results in a 78 gram or 14% increase in weight from the FF18 to the FF19 system. This is not a significant amount, as it only makes up approx. 0.1% of the total vehicle weight, or 0.05% of the combined vehicle and driver weight.

5.1.2 Driver Experience

During vehicle testing performed as part of the pre-master project of which this master thesis is based, the test drivers, Jennifer Nguyen and Robin Solheim made some notes about the feel of the FF18 steering system. They reported that the FF18 car was difficult to control precisely, and "scary" to drive (these notes were made during tests in which the drivers drove across a load testing ramp at speed, which likely contributed to the experience feeling "scary"). Little to no testing of FF19 and its steering system has been performed by the same drivers, and so it is not possible to get a comparison of the "feel" of the steering without the differences between each drivers subjective experience obscuring the evaluation.

However, it is still worth noting the experience of the FF19 driver in and on its own. The FF19 driver, Tania Bonilla, has through the course of the testing period once reported an issue with the steering system. This instance was when two of the roller pins bent, as described in 3.7.4. The drivers experience of the situation was that she was at one point not able to continue turning the steering wheel to get to a desired cornering radius. She pulled the wheel hard in the opposite direction, and was able to regain control of the steering. However, after this occurrence the steering required a higher effort to manoeuvre. It was at this point the bent rollers were discovered.

Neither before or after this occurrence (after which measures were taken to prevent similar issues) did the driver report any issues with the steering. At SEM19 she reported the feel of the steering to be comfortable and easy to manoeuvre. This stands in contrast to the experiences of FF18 test drivers Jennifer Nguyen and Robin Solheim.

The most obvious difference between the feel of the FF19 and FF18 steering is that the FF19 steering achieves the same range of cornering radii within a

180° rotation of the the steering wheel instead of a 90° rotation. This should increase the perceived precision of the steering.

In addition to the general "feel" of the steering, the amount of play should be noted. The SEM regulations states "Organisers will verify that steering is precise, with no play." [1]. The word "play" was interpreted during the development process as the backlash when reversing the direction the steering wheel is turned. There were made no precise measurements of the amount of backlash in FF18. However, the authors' recollection dictates that the FF18 steering system was perceived to have significantly more backlash than the FF19 steering system. Yet, during technical inspection at SEM19 one of the inspectors questioned the amount of play in the FF19 steering system. The inspector did not appear to be checking the amount of backlash when prompting this concern, but rather holding one wheel at a set steering angle, and seeing how much further he could pull the steering wheel. Thus, by play he referred to the stiffness of the system. According to the team members who were present he pulled very hardly, in spite of the self aligning loads on the steering during actual cornering being quite small (3.6.2). Eventually, the inspector called on a second inspector to verify. The second inspector had no concerns with the system at all, and so it was allowed to pass inspection.

5.1.3 Issues

After one track attempt at SEM19, one of the screws securing the alu block holding two of the rollers to its sliding alu flat bar had come loose. The failure of the screw had not led to further consequences, as the other screw was still in place. The screws in question were M3 screws, fastened to a threaded hole in the sliding alu flat bar. These threads were in poor condition, which was not surprising seeing as they were small threads in a soft material which had been assembled and disassembled many times. The issue was addressed by adding a steel nut to the back of all of these screws, in addition to rich amounts of thread locker.

During tight cornering at SEM19, a scraping sound was heard by the driver. It was hypothesised that this could come from the tie-rod/steering arm connection coming into contact with the rim, due to high deformations of the rim and/or steering arm. This issue was addressed by lowering the connection point by approx 10 mm, and grinding down the edge of the carbon fibre rim, to remove any excess flange width. After lowering the connection points the front wheels had to be re-aligned. The team was unable to complete any further track attempts after these adjustments, due to drive-train issues. Hence, it remains unknown whether the tie-rods caused the scraping sound and whether the adjustments were effective.

5.2 Suspension System

5.2.1 Weight and Moment of Inertia

Weight

The weight of the pins and brackets securing the suspension system to the wheel well was excluded in this comparison, as they were reused and did not cause a difference in weight between the FF18 and FF19 systems. The main differences in weight between the FF18 and FF19 systems were as follows:

- The shock absorber used in FF18 was replaced by a carbon fibre tube in the FF19 model, reducing weight.
- The length of the suspensions arms had to be increased in the FF19 model in order to fit in the FF19 wheel well, increasing weight.
- The brake discs in FF18 were swapped with thinner and slightly smaller brake discs in FF19, reducing weight.
- The aluminium wishbone arms in FF18 was swapped with carbon fibre tubes, reducing weight.
- The axle diameter was reduced from 20 mm in FF18, to 17 mm in FF19. Further reducing the size of the bearings and therefore also the width of the steering knuckle. Reducing weight.
- The steering knuckle in FF19 had to be lengthened, in order to fit the brake disc at the rear of the steering knuckle, increasing weight.

The weight of the FF18 suspension arms and shock absorber was 611 grams per unit. The weight of similar components in FF19 was 384 grams per unit. The weight of the steering knuckle assembly, including bearings, brake discs and steering arms was 1488 grams in the FF18 version and 1142 grams in the FF19 version. This results in a weight reduction of 25%, or a total reduction of 1039 grams counting both units. This translates to approximately 1.4% of the total weight of the vehicle.

Moment of Inertia

The moment of inertia of rotating components was computed from the CAD files in Fusion 360. It does not include the moment of inertia of the ball bearings, as the bearings used in the FF18 model are of an unknown type, and thus the data is not available.

The moment of inertia of the FF18 spindle was found to be $1.78 * 10^{-3} \text{ kgm}^2$, while the moment of inertia of the three piece spindle of the FF19 system, including the spacer, pin, screw and washer was found to be $1.08 * 10^{-3} \text{ kgm}^2$. A reduction of 40%, or $1.41 * 10^{-3} \text{ kgm}^2$ in total for both units.

The moment of inertia of the brake disc used in FF18 was found to be $5.39 * 10^{-3} \text{ kgm}^2$, while the ones used in FF19 had a moment of inertia of $2.19 * 10^{-3} \text{ kgm}^2$. A reduction of 59%, or $6.4 * 10^{-3} \text{ kgm}^2$ in total for both units.

Total Reduction

Let's assume a wheel diameter of 580 mm, and a speed of 30 km/h. In this case the wheels are spinning at:

$$\omega = \frac{30 \text{ km/h}}{3.6 \frac{\text{km/h}}{\text{m/s}}} / (0.558 \text{ m}/2) = 28.7 \text{ rad/s} \quad (5.1)$$

The kinetic energy held by the FF18 system at that speed is given by.

$$KE = \frac{1}{2} m_{FF18 \text{ suspension system}} v^2 + \frac{1}{2} I_{FF18 \text{ spindle and brake disc}} \omega^2 \quad (5.2)$$

$$= \frac{1}{2} * 2.10 \text{ kg} * \left(\frac{30}{3.6} \text{ m/s}\right)^2 + \frac{1}{2} * 7.17 * 10^{-3} \text{ kgm}^2 * (28.7 \text{ rad/s})^2 \quad (5.3)$$

$$= 75.9 \text{ J} \quad (5.4)$$

The kinetic energy held by the FF19 system at that speed is given by.

$$KE = \frac{1}{2} m_{FF19 \text{ suspension system}} v^2 + \frac{1}{2} I_{FF19 \text{ spindle and brake disc}} \omega^2 \quad (5.5)$$

$$= \frac{1}{2} * 1.53 \text{ kg} * \left(\frac{30}{3.6} \text{ m/s}\right)^2 + \frac{1}{2} * 3.27 * 10^{-3} \text{ kgm}^2 * (28.7 \text{ rad/s})^2 \quad (5.6)$$

$$= 54.5 \text{ J} \quad (5.7)$$

Swapping both units therefore reduced the kinetic energy of the vehicle at 30 km/h by 42.8 J, the equivalent of reducing the weight of a static component by $2 * KE/v^2 = 2 * 42.8 \text{ J} / \left(\frac{30}{3.6} \text{ m/s}\right)^2 = 1.23 \text{ kg}$. Approximately 1.6% of the vehicles total weight.

5.2.2 Issues

Before any track attempts were made at SEM19, one of the glued connections showed severely poor adhesion. A tube-end came apart from its tube under no other load than the weight of the system and wheel, as the car was lifted onto a stand. This failure of adhesion was surprising, as taking similar glued tube/tube-end connections apart had earlier showed difficult, even when using a heat-gun at high temperatures and a vice. None of the remaining connections showed signs of poor adhesion. However, as a safety measure, all the glued connections were reinforced with an M5 screw mounted through the tubes and tube-ends. This operation was assisted by team member David Guerrero.

The screw holding the brake disc mount and axle together on one of the spindles was found to be slightly loosened on two occasions during SEM19, despite having been secured with thread locker. The axle was still held together, though not as firmly. No measures were taken, apart from cleaning, re-applying thread locker and re-tightening slightly more firmly. As the screw also controls the pre-load on the bearings there was hesitance against tightening it too much.

Chapter 6

Discussion

6.1 Success of Project

The overall mission of DNV GL Fuel Fighter is to "Develop and build an ultra-efficient UrbanConcept car that excels in Shell Eco-marathon". During SEM19 each team was provided four attempts, spaced over four track sessions over the course of two days. This took place after four days of inspections and testing. The FF19 UrbanConcept car performed its best result during the second attempt at SEM19 of 181 km/kWh, beating the previous FF record of 176 km/kWh (which secured second place during SEM18). The result placed the team in second place after the end of day one. It was believed that significant improvements could be made in driving strategy. However, the leading team was far ahead, with a best result after day one of 231 km/kWh. In order to stand a chance of catching up the leader it was decided to swap to a newly designed gear system that had never been tested. The last minute installation led to technical difficulties, hindering the team from achieving any further results. The result of 181 km/kWh in day one was pushed from second place down to fifth place during day two, as other teams improved their results. The team in second place ended up with a best result of 192 km/kWh, 6% ahead of FF, while third and fourth place were 3 and 2% ahead respectively.

Though ending up in fifth place out of the 14 teams that made it through inspection is not a bad result, the FF team did not feel as if the mission of excelling at SEM had succeeded. Optimism was still instilled by the fact that FF was the only team among the top five with a brand new vehicle design, leaving less time for testing, tuning and driver practice. The author firmly believes that with more preparation the current vehicle design has the potential to take first place in SEM20.

6.1.1 Steering System

The main goal of the steering system development was to develop a new steering system that provides the designer full control of the steering geometry. The system was required to be direct and mechanical, while accomplishing a minimal turning radius of 6 m or less. Additionally the system needed to allow interaction with electronic actuators to enable autonomous control.

The design of the FF19 chassis attempted to position the driver as far to the front of the vehicle as possible to allow long lines in the rear section of the vehicle, in order to achieve low drag. The design also worked on minimising the projected frontal area of vehicle. For the purposes of steering system development this entailed that the system needed to fit in a very limited space, without interfering with other components or being in the way of the driver.

The final constructed design is in fact a direct mechanical system that allows the designer to control the steering geometry to any desired function. It's minimum turning radius was measured as less than 6 m, and the system is mounted in a way that leaves space for the mounting of-/ interaction with autonomous actuators. The system fits in the vehicle without interfering with other components, and the driver has been able to enter, exit and operate the vehicle without the system coming in her way.

In terms of fulfilling the requirements set for the system in 3.1, the project has succeeded on every account. The steering system made it through SEM19 without failure. Although some issues did arise during the course of the competition week, the steering remained fully functional. Still, even though the design did succeed in fulfilling requirements, there does not exist sufficient data to claim that it is in fact able to reduce the energy consumption of the vehicle. Future work on proving the efficiency of the design, and improving it to meet the encountered issues must be performed if the design is to see continued use.

The DNV GL Fuel Fighter vision statement, to "Inspire a sustainable future – through learning and creating innovative solutions that challenge today's perception of transportation." is one that is difficult to measure in absolute terms. During the course of SEM19, many members from other teams, Shell representatives and other observers came to the FF paddock area to have a closer look at the car. The interest that was taken in the steering system was intense. Passers by were constantly stopping to ask about how it worked and how it was designed. Many asked to take photos. No other component or system in the vehicle received nearly as much attention during the week spent at SEM19. Based on this, one might assume that the design succeeded in inspiring the crowd at SEM.

6.1.2 Suspension System

The objective of the suspension system is to suspend the front wheels in a stable manner, avoiding excessive rolling resistance. This needs to be done without interfering with steering geometry and without compromising other parts of the vehicle. The decision to opt for a non-dampened suspension was a risky one at that, as a non dampened vehicle will receive more intense shocks from uneven road surfaces. This could cause driver discomfort or component failure, both in the suspension and in other parts of the vehicle.

The experience from SEM19 shows that the developed system managed to fulfil its objective, with no evidence of high bump loads affecting the vehicle, and no complaints from the driver. The carbon fibre tubes making out the suspension arms proved to have sufficient strength to make it through SEM19, and the system had sufficient flexibility to not cause shocks large enough to damage the suspension or vehicle.

Of the two issues discovered with the suspension during SEM19, one was quickly treated, and no further signs of this issue was seen during the competition period. The other issue was never solved, and so some rework is required to ensure a system safe from failure.

The system has proved that designing for zero sweep radius without the use of camber or steering axis inclination is possible within the boundaries of the surrounding components in FF19. The design has also ensured an axle/bearing setup that provides a significant increase in the axial distance between each bearing groove. This increases the capability to withstand bending moment, and reduces the loads on the rear bearing groove, which in theory reduces rolling resistance. A camber free design also ensures low rolling resistance, and the absence of camber and steering axis inclination reduces the number of factors interfering with the steering geometry. No problems with instability of the front wheels has been experienced, suggesting that the positive caster angle of 3° has been sufficient.

This has all been achieved while reducing the kinetic energy of the system by 28%. Success in the objective of developing a new front suspension has therefore been achieved, yet more testing is needed to determine solid proof of its efficiency, and some improvement is crucial to ensure safe operation in the future.

6.2 Review of Process

6.2.1 Initial Phase

In the case of both the steering and suspension system developments, the initial phases were characterised by a very structured and organised approach.

Time and effort was put into creating an overview where as many factors, solutions and doorways to further solutions were considered as possible. This structure was laid down for the author to force himself not to land on a decision too early, or to become too blinded by one particular solution to not see potential in other solutions.

Still, it did not take too long for the author to start favouring specific solutions. Especially in the case of the steering system development, the DGW was favoured quite early. Though the differences between its ability to obtain perfect Ackermann steering and that of a traditional system might not be very substantial, it was favoured in part from a desire to create something unseen. The author had a strong desire to come up with a solution that gives new possibilities, and is not just another iteration of a two hundred year old system.

In the case of the suspension system, specific solutions were not favoured as early. In stead, decisions were made no earlier than the time constraint of the project required them to be.

6.2.2 Further Development Phase

In the case of the steering system development, the process continued into further development in a structured manner. Several different types of prototypes were made and tested to ensure the feasibility of the concept, and to find ways to make it operate smoothly.

In the case of the suspension system development, the further development was made quite hastily. Especially since an important factor in the suspension system design is weight, more time should have been put into the dimensioning of the system, had that time been available. Perhaps the weight could have been minimised further, or perhaps the haste-full dimensioning could have caused some features to be under-dimensioned. Still, the time constraint hindered more effort to be put into the dimensioning, and even with such a haste-full process the system was finished at the last minute before departure to SEM19, leaving no time for testing at speed.

6.2.3 Production Phase

The production of the steering system was done in a trial and error type approach. Apart from the DGW that had to be CNC-milled, the parts were 3d-printed or cut from CFRP tubes and alu rails. This meant many iterations of the design could be made, tested, and improved upon in a short manner of time.

The suspension on the other hand consisted of a much greater number of parts, most of which had to be machined, and most of which required three or more machining processes. This production was highly time consuming.

Although assistance in production was given by several team members on a few occasions, the vast majority of these parts were made by the author alone. Thus the production phase required more time than what had been hoped for. An important take-away from this part of the process is to plan for delays in production, leave more time for testing, and ask for assistance by available team members sooner when necessary.

6.2.4 Conclusions

In hindsight, some processes should have been started earlier, especially those in the suspension system development. More assistance should have been acquired from available team members, and more time should have been left for testing and validation. The author has experienced feeling heavily overworked during the majority of the process, and perhaps developing two new critical vehicle systems from scratch should have been a two-person job. Still, the author feels that it was important that those two systems be developed in tight coherence with each-other, and so does not regret accepting responsibility for both systems. The author concludes that even though setting off time for a well structured and thorough initial phase is important, one should not linger in this phase for too long before commencing in further development. In spite of the time constraint and difficulties, both systems were produced, assembled, mounted and functional by the time of the competition at SEM19.

6.3 Future Work

6.3.1 Steering System

Necessary Improvements

The concern about play proposed by the technical inspector at SEM19, mentioned in 5.1.2 should be addressed. It is not clear whether it was the inspector or the author who misinterpreted the meaning of the word "play" in the SEM regulations, though interpreting play as backlash seems to the author to be the most common interpretation among online sources (e.g. [30]). Several of the inspectors seemed lacking of technical knowledge. For instance one team experienced the brake inspector unable to understand the rules of the brake system. He supposedly had to ask the team members what the "N" in "A parking brake function is required ... It must provide a brake force of at least 50 N." [1] meant. Regardless of whether or not the issue was due to the inspectors understanding of the rules, steps should be taken to assure the system is perceived as having both very little backlash **and** deformation.

The component in the system with the most amount of free length, and which appears to deform the most when load is applied to the steering is the steering arms. Because of the height of the steering system placement, these arms have a high length in the vertical direction. This is also relevant to the scraping issue discussed in 5.1.3. In addition to the high free length making the arms prone to deformation, the high placement also positions them closely to the rim. A suggested improvement of the system would therefore be to find a way of reducing the vertical length of the steering arms.

For further improved feel of the system, and reduction of backlash, one might also consider improving the way the sliding steering components are mounted. Perhaps linear bearings or rails could be used to hold the sliding parts more firmly in place without hindering axial movement.

Another proposed improvement which could simplify the design and reduce space consumption and weight would be to remove the off-setters, but rather allow the sliding parts of the steering to connect with the tie-rods along different axes on each wheel (due to one sliding part being in front of the DGW, and the other to the rear of the DGW). The un-aligned axes could be compensated for in the functions that define the guide curves, so that this change would not affect steering geometry.

Validation

In order to prove whether or not the wheels actually follow the desired steering geometry this should be measured. This could be done in a number of ways, for example rolling the vehicle onto its side, placing a digital level onto each wheel, and seeing whether the angles correspond. Preferably a method of measuring at speed under load should be devised as well. The effect of poor steering geometry could be evaluated by building a rig that holds the wheels with adjustable load and adjustable toe, then using a load cell to measure the rolling resistance on the rig at different loads and amounts of toe when placed on e.g. a treadmill.

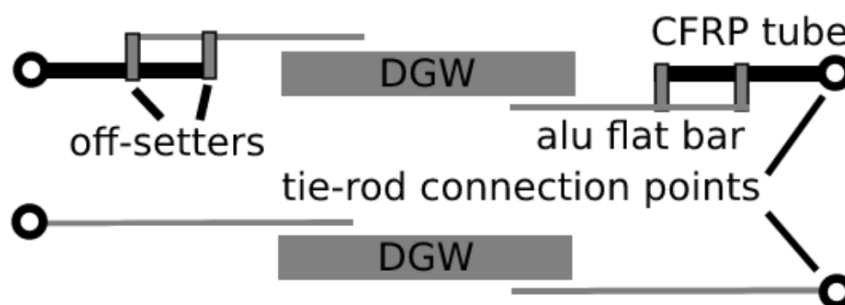


Figure 6.2: Sketch of the steering system with and without off-setters, seen from above.

It was the hopes of the author that the telemetry data from SEM19 would be comparable to the data from SEM18, so that some conclusions could be drawn from these sets. Specifically, the rate of kinetic energy loss when coasting through a corner, vs. in a straight line. Unfortunately, the track was changed from SEM18 to SEM19, meaning every corner had different cornering radii, and every portion of the track had different slope and different asphalt quality. Hence, the data is not able to provide a basis for any conclusions regarding improvements in cornering losses. These types of data could however be gathered by setting up a test track and driving through it multiple times with different setups installed.

In the current steering system, perfect Ackermann geometry was used. However, as discussed in 2.3, this is not necessarily the optimal geometry. Test setups such as those described above could be used to test different steering geometries in order to determine optimal ratios. Being able to determine an optimal geometry, and swapping only the DGW to immediately provide this geometry is after all the most significant advantage of the DGW system.

6.3.2 Suspension System

Necessary Improvements

The issue of the loosened axle screw (5.2.2) needs to be solved, either by devising a way of securing the screw, or replacing it by another fastening mechanism. E.g. a lock ring could be used, however this would not allow adjustment of the pre-load on the bearings, and it might be difficult to achieve perfect fit. Another alternative could be locking the tightening screw in the desired position, e.g. using a pin through a hole in the screw head and a locating feature on the brake disk mount.

Additionally, the issue with the poor glue adhesion on one of the tube-ends should be investigated further, to discover if this could be a repeated issue. If so, the added strength from the screws through the tubes and tube-ends should be evaluated.

Validation

Measures should be taken to evaluate the suspension set-up. Most of the time during this project was spent on conceptual design, and so some factors needed to be decided based on assumptions. The selected caster angle of 3° is one factor that should be evaluated, e.g. by creating a testing suspension that allows caster angle adjustments, so that different angles can be tested. This will help find the perfect middle-ground between stability at speed, and steering effort. The same rig could be used to adjust camber and SAI, to validate the zero camber design. The current suspension is mounted with zero camber under no load, deformation under load could cause some camber,

and so testing should also be performed to identify which camber setting under no load results in zero camber under relevant loads.

The effects of bearing pre-load on rolling resistance should also be measured, to identify the optimal amount. This could be done by mounting both suspensions to a rig placed on a treadmill, and measure the load on the rig using a load cell. The amount of pre-load must be sufficient to hold the spindle firmly against the bearings, but not excessive so as to cause dramatic increases in resistance.

Appendix A

Ackermann System vs. Perfect Ackermann Geometry

We'll seek to discover to what extent the steering geometry provided by the traditional Ackermann system deviates from the perfect Ackermann geometry. x represents the movement of the tie rod between the two steering arms in figure A.1.

Thus:

$$x = -l_{sa} [\sin(\beta + \gamma_i) - \sin(\beta)] \quad (\text{A.1})$$

$$x = l_{sa} [\sin(\beta - \gamma_o) - \sin(\beta)] \quad (\text{A.2})$$

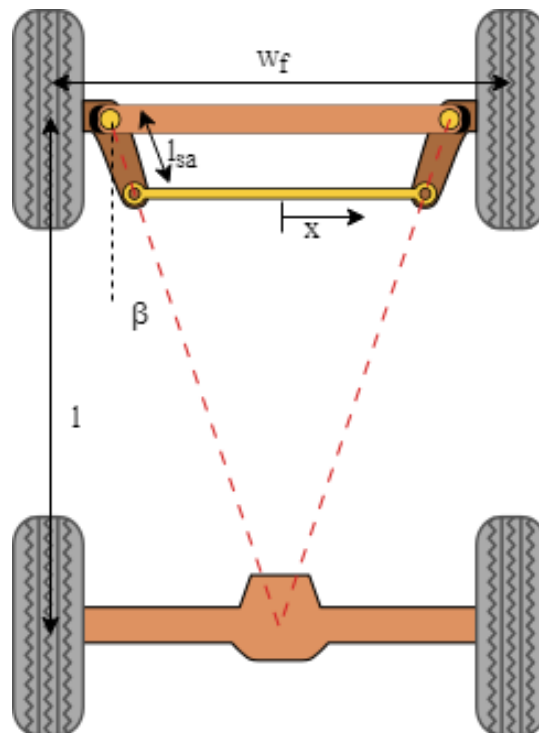


Figure A.1: Traditional Ackermann steering system

Solving A.1 with A.2 gives:

$$\sin(\beta) - \sin(\beta + \gamma_i) = \sin(\beta - \gamma_o) - \sin(\beta) \quad (\text{A.3})$$

$$\sin(\beta - \gamma_o) = 2 * \sin(\beta) - \sin(\beta + \gamma_i) \quad (\text{A.4})$$

$$\gamma_o = -\sin^{-1}[2 * \sin(\beta) - \sin(\beta + \gamma_i)] + \beta \quad (\text{A.5})$$

Norris Williams stated in 1906 that the steering arm angle β should be such that the continued line of the of the two steering arms intersect in the centre of the rear axle[20][pg.64]. Thus, $\beta = \tan^{-1}(\frac{w_f/2}{l})$. With the dimensions of FF19 this results in $\beta = 17.7^\circ$.

Combining 3.1 and 3.2 we get

$$\gamma_o = \tan^{-1}\left(\frac{l}{\frac{l}{\tan(\gamma_i)} + w_f}\right) \quad (\text{A.6})$$

in which l and w_f are the wheelbase and track-width of the car. In the case of FF19 these are 1745 and 1115 mm. Figure A.2 plots the outer wheel steering angle as a function of inner wheel steering angle considering the dimensions of FF19. The green line (lower) represents the perfect Ackermann geometry, as defined by equation A.6, while the red line (middle) represents the resulting steering geometry from utilising the traditional Ackermann system in FF19, as defined by equation A.5. The blue line represents the diagonal, in which the steering angle of each wheel is identical.

When observing inner wheel steering angles from 0 to 23° (equivalent of a 5.5 m turn radius with FF19 dimensions), the maximum deviation between the perfect Ackermann geometry and the traditional Ackermann geometry is 1.52° . Yet, it is worth noting that the deviations can be reduced drastically by increasing the steering arm angle from what Norris Williams dictates. This results in almost negligible deviations within the required range of cornering radii.

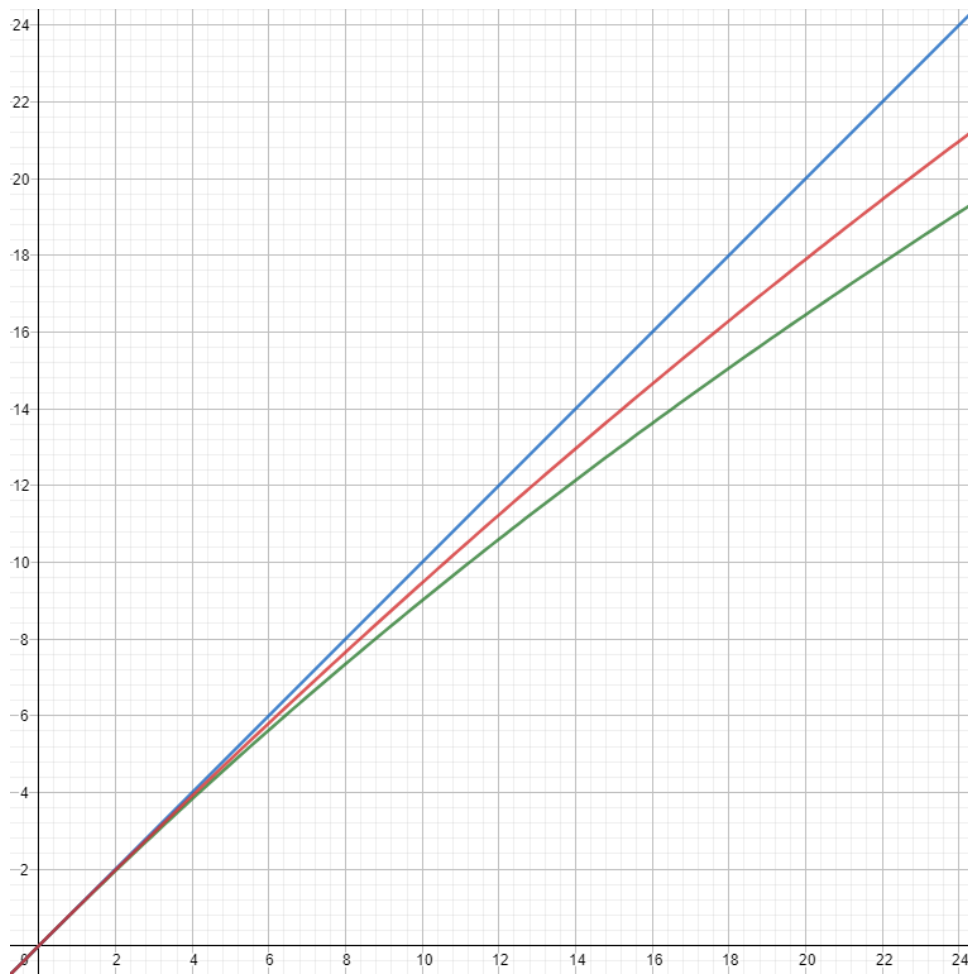


Figure A.2: Comparison of perfect Ackermann geometry and the steering geometry of the traditional Ackermann system if utilised in FF19.

Appendix B

Risk Assessment Form

Please note that the attached risk assessment is written in Norwegian.



ID	30947	Status	Dato
Risikoområde	Risikovurdering: Helse, miljø og sikkerhet (HMS)	Opprettet	11.12.2018
Opprettet av	Lars Røed Ramstad	Vurdering startet	11.12.2018
Ansvarlig	Lars Røed Ramstad	Tiltak besluttet	
		Avsluttet	11.12.2018

Risikovurdering:**Risikovurdering Prosjektarbeid****Gyldig i perioden:**

9/1/2018 - 6/11/2019

Sted:

Trondheim

Mål / hensikt

Hensikten med denne vurderingen er å avdekke potensiell risiko involvert med gjennomføringen av forfatterens prosjekt/master arbeid, og om nødvendig inverterte tiltak for å begrense nevnte risiko.

Bakgrunn

Risikovurderingen utføre i henhold til standard prosedyre for eksperimentelt arbeid ved NTNU.

Beskrivelse og avgrensninger

Aktiviteter inkluderer bruk av verktøy ved MTP's realiseringslab, inkludert både håndverktøy og maskiner omfattet av MTP's krav til HMS opplæring. I tillegg inkluderer vurderingen risiko ved testing av komponenter og kjøretøy, både i og utenfor labben. mponent testing in- and outside of the workshop.

Forutsetninger, antakelser og forenklinger

Assumptions are made that machines and equipment at the lab are properly maintained and functional, and that other users in the workshop are trained in and follow the HSE guidelines given by MTP.

Det antas at maskiner og utstyr ved realiseringslabben er godt vedlikeholdt og at andre brukere ved labben har og benytter seg av HMS opplæringen gitt ved MTP.

Vedlegg

[Ingen registreringer]

Referanser

[Ingen registreringer]

11/12-18




Oppsummering, resultat og endelig vurdering

I oppsummeringen presenteres en oversikt over farer og uønskede hendelser, samt resultat for det enkelte konsekvensområdet.

Farekilde: Maskinverktøy


Uønsket hendelse: Små kutt

Konsekvensområde: Helse

Risiko før tiltak:  Risiko etter tiltak: 

Uønsket hendelse: Klemskader

Konsekvensområde: Helse

Risiko før tiltak:  Risiko etter tiltak: 

Uønsket hendelse: Sponsprut i øyne

Konsekvensområde: Helse

Risiko før tiltak:  Risiko etter tiltak: 

Farekilde: Bruk av tungt utstyr og materialer

Uønsket hendelse: Klemming av lemmer under tung gjenstand

Konsekvensområde: Helse

Risiko før tiltak:  Risiko etter tiltak: 

Farekilde: Bruk av sveiseapparat/plasmabrenner o.l.

Uønsket hendelse: Brannskade

Konsekvensområde: Helse

Risiko før tiltak:  Risiko etter tiltak: 

Farekilde: Testing av kjøretøy

Uønsket hendelse: Kollisjon

Konsekvensområde: Helse

Risiko før tiltak:  Risiko etter tiltak: 

Ytre miljø

Risiko før tiltak:  Risiko etter tiltak: 

Materielle verdier

Risiko før tiltak:  Risiko etter tiltak: 

Endelig vurdering



Det eksisterer som alltid risiko for helse ved bruk av kraftige verkstedmaskiner. Forhåndsiltak som aktsom bruk og korrekt anvendelse av verneutstyr kan ikke fullstendig utelukke disse, og fortløpende vurderinger av risiko må derfor utføres ved utførelse av ethvert arbeid.

Ettersom prosjektet kun konstruerer lette kjøretøy begrenset til svært lav hastighet er fare for helse og ytre miljø lav. Eget materielt utstyr kan derimot lett skades, og ved ethvert eksperiment bør nytteverdien vurderes opp mot risikoen for slike skader.

Involverte enheter og personer

En risikovurdering kan gjelde for en, eller flere enheter i organisasjonen. Denne oversikten presenterer involverte enheter og personell for gjeldende risikovurdering.

Enhet /-er risikovurderingen omfatter

- NTNU

Deltakere

Lesere

[Ingen registreringer]

Andre involverte/interessenter

[Ingen registreringer]

Følgende akseptkriterier er besluttet for risikoområdet Risikovurdering: Helse, miljø og sikkerhet (HMS):

Helse



Materielle verdier



Omdømme



Ytre miljø



Oversikt over eksisterende, relevante tiltak som er hensyntatt i risikovurderingen

I tabellen under presenteres eksisterende tiltak som er hensyntatt ved vurdering av sannsynlighet og konsekvens for aktuelle uønskede hendelser.

Farekilde	Uønsket hendelse	Tiltak hensyntatt ved vurdering
Maskinverktøy	Små kutt	
	Klemskader	Bruk av tettsittende tøy og fravær av hansker, løse tråder o.l.
	Klemskader	Bruk av tettsittende tøy, samt fravær av hansker
	Sponsprut i øyne	Bruk av vernebriller
Bruk av tungt utstyr og materialer	Klemming av lemmer under tung gjenstand	Bruk av vernesko med ståltupp
Bruk av sveiseapparat/plasmabrenner o.l.	Brannskade	Bruk av sveisefrakk og maske
Testing av kjøretøy	Kollisjon	Ikke utfør testing på trafikkerte områder
	Kollisjon	Benytt fempunkts setebelte i bilen
	Kollisjon	Ikke utfør testing på trafikkerte områder
	Kollisjon	Benytt fempunkts setebelte i bilen

Eksisterende og relevante tiltak med beskrivelse:

Bruk av vernebriller

-

Bruk av tettsittende tøy, samt fravær av hansker

-

Bruk av vernesko med ståltupp

-

Ikke utfør testing på trafikkerte områder

-

Benytt fempunkts setebelte i bilen

-

Bruk av sveisefrakk og maske

-

Risikoanalyse med vurdering av sannsynlighet og konsekvens

I denne delen av rapporten presenteres detaljer dokumentasjon av de farer, uønskede hendelser og årsaker som er vurdert. Innledningsvis oppsummeres farer med tilhørende uønskede hendelser som er tatt med i vurderingen.

Følgende farer og uønskede hendelser er vurdert i denne risikovurderingen:

- **Maskinverktøy**
 - Små kutt
 - Klemskader
 - Sponsprut i øyne
- **Bruk av tungt utstyr og materialer**
 - Klemming av lemmer under tung gjenstand
- **Bruk av sveiseapparat/plasmabrenner o.l.**
 - Brannskade
- **Testing av kjøretøy**
 - Kollisjon

Detaljert oversikt over farekilder og uønskede hendelser:

Farekilde: Maskinverktøy

Uønsket hendelse: Små kutt

Sannsynlighet for hendelsen (felles for alle konsekvensområder):

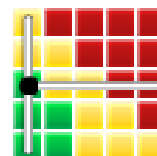
Sannsynlig (3)

Kommentar:

[Ingen registreringer]

Konsekvensområde: HelseVurdert konsekvens: **Liten (1)**

Kommentar: [Ingen registreringer]

Risiko:**Uønsket hendelse: Klemskader**

Sannsynlighet for hendelsen (felles for alle konsekvensområder):

Svært lite sannsynlig (1)

Kommentar:

[Ingen registreringer]

Konsekvensområde: HelseVurdert konsekvens: **Stor (3)**

Kommentar: [Ingen registreringer]

Risiko:

**Uønsket hendelse: Sponsprut i øyne**

Sannsynlighet for hendelsen (felles for alle konsekvensområder):

Svært lite sannsynlig (1)

Kommentar:

[Ingen registreringer]

Konsekvensområde: Helse

Vurdert konsekvens: **Svært stor (4)**

Kommentar: [Ingen registreringer]

Risiko:



**Farekilde: Bruk av tungt utstyr og materialer**

Uønsket hendelse: Klemming av lemmer under tung gjenstand

Sannsynlighet for hendelsen (felles for alle konsekvensområder):

Lite sannsynlig (2)

Kommentar:

[Ingen registreringer]

Konsekvensområde: Helse

Vurdert konsekvens: **Middels (2)**

Kommentar: [Ingen registreringer]

Risiko:



**Farekilde: Bruk av sveiseapparat/plasmabrenner o.l.**

Uønsket hendelse: Brannskade

Sannsynlighet for hendelsen (felles for alle konsekvensområder):

Lite sannsynlig (2)

Kommentar:

[Ingen registreringer]

Konsekvensområde: Helse

Vurdert konsekvens: **Middels (2)**

Kommentar: [Ingen registreringer]

Risiko:



Farekilde: Testing av kjøretøy

Uønsket hendelse: Kollisjon

Sannsynlighet for hendelsen (felles for alle konsekvensområder): **Sannsynlig (3)**

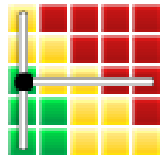
Kommentar:

[Ingen registreringer]

Konsekvensområde: Helse

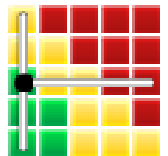
Vurdert konsekvens: **Liten (1)**

Kommentar: [Ingen registreringer]

Risiko:**Konsekvensområde: Ytre miljø**

Vurdert konsekvens: **Liten (1)**

Kommentar: [Ingen registreringer]

Risiko:**Konsekvensområde: Materielle verdier**

Vurdert konsekvens: **Middels (2)**

Kommentar: [Ingen registreringer]

Risiko:



Oversikt over besluttede risikoreducerende tiltak:

Under presenteres en oversikt over risikoreducerende tiltak som skal bidra til å reduseres sannsynlighet og/eller konsekvens for uønskede hendelser.

Detaljert oversikt over besluttede risikoreducerende tiltak med beskrivelse:



Detaljert oversikt over vurdert risiko for hver farekilde/uønsket hendelse før og etter besluttede tiltak

Bibliography

- [1] Shell. *Shell Eco–Marathon 2019 Official Rules*. 2018.
- [2] Shell. *Shell Eco–Marathon 2018 Official Rules*. 2018.
- [3] Richard Stone and Jeffrey K. Ball. *Automotive Engineering Fundamentals*. SAE International, 2004.
- [4] Department of the Army. *TM 9-8000 Principles of Automotive Vehicles*. 1985.
- [5] William H. Crouse. *Automotive Mechanics*. McGraw-Hill, 1965.
- [6] Pei-Shi Huang and Alfred Pruckner. *Steer by Wire, in: Steering Handbook*. 2017.
- [7] Thomas D. Gillespie. *Fundamentals of Vehicle Dynamics*. SAE International, 1992.
- [8] Sadjyot Biswal, Aravind Prasanth, M S Dhiraj Sakhamuri and Shaurya Selhi. *Design and Optimization of the Steering System of a Formula SAE Car Using Solidworks and Lotus Shark*, 2016.
- [9] J. Bernard D. Isler P. Kobler F. Kolb N. Weidmann L. Guzella J.J. Santin, C.H. Onder. *The World's Most Fuel Efficient Vehicle - Design and Development of PAC-car II*. vdf, 2007.
- [10] Hans Pacejka. *Tire and Vehicle Dynamics*. 2012.
- [11] Brad Kerr Tim Dunn, Kevin Jesser and Robert Mann. *Automotive Light Vehicle Level 2*. Jones and Bartlett Learning, 2014.
- [12] Richard G. Budynas and J. Keith Nisbett. *Shigley's Mechanical Engineering Design*. McGraw-Hill, 2011.
- [13] Brian M. Kennedy, Durward K. Sobek and Michael N. Kennedy. *Reducing Rework by Applying Set-Based Practices Early in the Systems Engineering Process*, 2013.
- [14] Stephannie Houde et al. *Handbook of Human-Computer Interaction*, 1997.
- [15] Smith Stål. *Lagerkatalog*. 2019.
- [16] Lars Røed Ramstad. *Steering System and Load Case Development in DNV GL Fuel Fighter*. 2018.
- [17] Wasim Younis. *Up and Running with Autodesk Inventor Simulation*. 2010.

- [18] Gunnar Härkegård. *Dimensjonering av maskindeler*. Tapir akademisk forlag, 2004.
- [19] Fridtjov Irgens. *Formelsamling mekanikk*. Tapir akademisk forlag, 2010.
- [20] Norris Williams. *Modern Steam Road Wagons*. 1906.

Websites

- [21] DNV GL Fuel Fighter. <https://www.fuefighter.no/>. [Online; accessed 13-November-2018].
- [22] Shell. Shell Eco-Marathon. <https://www.shell.com/energy-and-innovation/shell-ecomarathon.html>. [Online; accessed 13-November-2018].
- [23] "Bromskloss". Ackermann. <https://commons.wikimedia.org/wiki/File:Ackermann.svg>, 2006. [Online; accessed 14-November-2018].
- [24] Techzilon Training Solutions. <https://www.techzilon.com/product/caeproject07-static-and-dynamic-analysis-of-wishbone-suspension-of-a-passenger-car/>. [Online; accessed 10-July-2019].
- [25] Suitability of rolling bearings for industrial applications. https://www.skf.com/binary/21-291479/0901d196805fd45c-1708-0021-EN---17000-w_tcm_12-291479.pdf. [Online; accessed 13-July-2019].
- [26] MatWeb: Aluminum 7075-T6. <http://www.matweb.com/search/DataSheet.aspx?MatGUID=4f19a42be94546b686bbf43f79c51b7d&ckck=1>. [Online; accessed 13-July-2019].
- [27] New World Encyclopedia: Aluminum. <https://www.newworldencyclopedia.org/entry/Aluminum>. [Online; accessed 13-July-2019].
- [28] MatWeb: Aluminum 6082-T6. <http://www.matweb.com/search/DataSheet.aspx?MatGUID=fad29be6e64d4e95a241690f1f6e1eb7&ckck=1>. [Online; accessed 17-July-2019].
- [29] The Physics Factbook. <https://hypertextbook.com/facts/2004/KarenSutherland.shtml>. [Online; accessed 17-July-2019].
- [30] Merriam-Webster Dictionary: backlash. <https://www.merriam-webster.com/dictionary/backlash>. [Online; accessed 17-July-2019].

